A Digital Maskless Photolithographic Patterning Method for DNA Based UV Photocleavable PEGDA Hydrogels with A Camphorquinone-Triethanolamine Photoinitiator

By

Wenlu Wang

A thesis submitted to Johns Hopkins University in conformity with the

requirements for the degree of Master of Science in Engineering

Baltimore, Maryland

May 2019

Abstract

The prerequisite of establishing Ultra Violet photo-responsive soft materials is to find out a suitable photoinitiator triggered by visible light. In this thesis, we introduced a blue-light-absorbing (peak absorbance at 470nm) photoinitiator system, camphorquinone and triethanolamine, to overcome the drawbacks of widely used UV photoinitiators that are incompatible with biomolecules like DNA and will crosstalk with UV photo-cleavable chemistry we utilized. We optimized the formulation to photopattern PEGDA-DNA co-polymerized hydrogel for high pattern fidelity and mechanical property to be isolated from microfluidic devices. Digital maskless photolithography enables the immobilization of acrylate-modified oligonucleotides within patterned hydrogels at a dimension of tens of microns. To demonstrate the control of UV photo-cleavage, we used an acrylate-modified DNA strand containing a 1-(2-nitrophenyl) ethyl spacer to selectively cleave and release oligonucleotide segments from a region inside a PEGDA hydrogel. This UV responsive co-PEGDA-DNA hydrogel fabrication approach can be used in performing pattern-transformation algorithms such as edge detection or as a trigger for downstream sequential release cascades on micron scale.

Committee members:

Advisor: Prof. Rebecca Schulman

Reader: Prof. Sung Hoon Kang

Acknowledgements

During my two years of master's research, I received generous help from many people. First, I want to say thank you for Prof. Schulman and Phillip Dorsey, they showed great patience and gave me insightful suggestions on how to overcome obstacles in experiments and their ideas made me understand the importance of rigidity and creativity in scientific research. I'm also very grateful to Misha, Rachal, Sisi, Lei and other group members, from discussion and collaboration with them, I learned a lot of techniques and how to think in a different angle. Finally, I would like to thank my family. It's their support and encouragement that inspired me to work hard and keep my passion to move on.

Table of Contents

List of figures

1, Introduction

1.1, DNA functionalities

1.1.1, Basic characteristics

DNA has long been known as a powerful genetic information carrier and as the translational code for the synthesis of proteins. Briefly, a double-stranded DNA molecule forms because of the Watson-Crick hybridization of two polynucleotide strands composed of monomeric units called nucleotides. Each nucleotide is composed of i) one of four nucleobases (cytosine [C], guanine [G], adenine [A] or thymine [T]), ii) a deoxyribose, and iii) a phosphate group. The backbone of polynucleotides is formed via covalent bonds, and the bases of the two separate strands are joint together, according to base pairing rules (A with T and C with G), by hydrogen bonds into a Watson-Crick double helix structure. Genetic and other kinds of information including substantial structural and functional information is encoded in the sequence of DNA bases [1]. These fundamental characteristics makes DNA an excellent engineering macromolecule not only because its biological nature enables applications in vivo, but also its programmable feature enables predictable molecular behavior by DNA sequence design [2]. Based on this, DNA have been used to develop logic gates, computational circuits, and chemical programming that are capable of implementing intricate algorithms with simple reactions [3].

Nowadays, more features of DNA are explored and exploited, making DNA a major class of natural macromolecules for designing functional materials [4]. Triple helix CGC^+ and TAT

are known and Soto et al found that the formation of triplexes CGC$^+$ and its transition to duplex are driven by environmental pH [5]. Another pH stimulated structure is the i-motif configurations, an assembly of C-rich strands into a four-stranded quadruplex structure. Similarly, the G-rich strand will transfer into G-quadruplex triggered by K$^+$ [6]. Metal ion-base interactions can stabilize DNA by forming metal ion bridges in some cases such as C-Ag$^+$-C or T-Hg^{2+}-T. Generally, these structures and motifs can be removed by counter signals, indicating reversible structural changes.

Other than structural motifs, DNA can act as aptamers that specifically recognize targets such as virus [7] and epithelial cell adhesion molecules [8]. DNA also possesses catalytic functions, for example, Travascio et al. found that DNA G-quadruplex aptamer/hemin complexes greatly enhanced the peroxidase activity compared with hemin alone [9,10].

1.1.2, Modifications for crosslinking with polymers: Acrydite

Due to its tunable multifunctionality, convenient programmability, adequate biocompatibility, and biodegradability, as well as its precise molecular recognition, DNA is esteemed by scientists for interfacing biology with material science to construct hydrogels with broad applications in the biomedical area. Luo et al. have successfully built pure DNA hydrogels from branched DNA building blocks with sticky ends, X- and Y- junctions [11]. Noll et al. developed a simplified strategy for DNA-based hydrogel that relies on the self-assembly of short linear double-stranded DNA building blocks with sticky ends [12]. However, pure DNA hydrogel preparation and production on a large scale is far too expensive. Thus, the most common thoughts to fabricate hydrogel with versatile functionality of DNA are integrating DNA strand onto the hydrogel backbone to form hybrid hydrogels.

DNA modification is required to cooperate with synthetic polymers such as polyacrylamide and PEGDA. Acrydite is a phosphoramidite that allows the synthesis
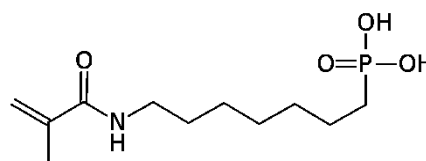
Acrydite structure

of oligonucleotides with a methacrylate group at the 5' end (less commonly 3' or internal). Acrydite-modified oligonucleotides can react with nucleophiles such as thiols (Michael addition chemistry). More importantly, Acrydite-modified oligonucleotides can be incorporated, stoichiometrically, into hydrogels such as polyacrylamide, using standard free radical polymerization chemistry, where the double bond in the Acrydite group reacts with other activated double-bond containing compounds.

1.1.3, Modifications for photo-sensitive reactions

Modification of the DNA backbone can also endow DNA with multiple functionalities. To design UV responsive materials, several Photo-active linkers have been developed including *o*- nitrobenzyl, azobenzene, and triphenylmethane. The *o*-nitrobenzyl ester was widely used for the study of photolability (photocleavage) because of its low degradation kinetics and fast decomposition at photoirradiation (3.5mW/cm^2, 365nm) comparing with 1-*o*-phenylethyl ester [13,14]. Another kind of UV photo-sensitive reagent is the azobenzene derivatives. This photosensitive molecule can isomerize between cis- and trans-state upon UV-Visible irradiation. When exposed to visible light, azobenzene is in trans-state and will induce DNA hybridization with complementary sequences, and this transition is reversible. UV photosensitive reactions have promising applications such as drug delivery, sensors, and soft robots. The spacer we used in this thesis is 1-(2-nitrophenyl) ethyl, a o-nitrobenzyl derivative.

1.1.4, Modifications for RGD peptides: SMCC/ Click chemistry

Peptide-oligonucleotide conjugates are constructed covalently linking DNA strand to synthetic peptide sequences. POCs are envisioned diverse applications in following areas: simultaneously control of multiple input signals, hierarchical self-assembly across multiple length scales, synthesis of functional proteins from synthetic peptide components, and artificial antibodies and active sites organized by DNA scaffolds. In this section, we will briefly introduce two approaches to POC fabrication: solid-phase synthesis of the entire hybrid molecules, and separate synthesis and then coupling. The first method is synthesizing peptides or oligonucleotides by protected monomers on a solid resin and then deprotecting and cleaving the entire hybrid strand off the resin. The drawback of this method is that the conditions for cleavage and deprotection are not compatible with the molecule because the strong acidity will damage oligonucleotides, therefore it's not commonly used. The second approach including the direct coupling of modified peptides and oligonucleotides and crosslinking two segments together by bifunctional linkers. In most cases, bifunctional linkers can react with thiol and amine on each end to connect oligonucleotides and peptides such as sulfo-SMCC, SPDP, and DBCO-maleimide. To mention that recently click chemistry has been widely utilized for bioconjugation for its high efficiency, minimal byproducts and low toxicity (azide and alkyne) [15].

1.2, DNA Stimuli-responsive hydrogels

As we mentioned in section 1.1, structural and functional information is encoded in the base sequence of nucleotides, therefore, when external stimuli such as pH, metal ions, light irradiation, force, or molecules are exerted, DNA can undergo structural changes. Such changes include i-motifs, triplex DNA, metal-ion-bridged duplexes, G-quadraplex, unzipping of DNA

hairpins or programmed hybridization. The integration of stimuli-responsive oligonucleotides with biopolymers to form a co-DNA-polymer hydrogel provides the opportunity to exploit the functional information in DNA strands as well as the specific properties of the polymer to yield stimuli-responsive hydrogels. These hydrogels have a variety of applications, such as drug delivery, biosensing, soft robots, tissue engineering, 3D cell culture, catalysis, etc.

pH-Responsive DNA hydrogels

pH-responsive DNA hydrogels are usually used as shape-memory hydrogels that undergo gel-to-solution transitions by the reversible DNA transition between original state and i-motif or triple complex structures when environmental pH changes. Guo et al copolymerized acrylamide with acrydite modified C-rich nucleotides to form a pH-responsive hydrogel. The C-rich strands can self-assemble into an i-motif at pH = 5 and dissociate to a random coil at pH = 8, leading to the transition of the hydrogel to a "quasi- liquid" state [16]. Wilson et al found that an anticancer drug Coralyne preferentially binds to TA•T triplex, and the release rate from hydrogel increased as triplex dissociates with pH changing from 7 to 10 [17], thus they can potentially be used in drug delivery.

Temperature-responsive DNA hydrogels

In most cases, thermosensitive DNA hydrogel always possesses multiple responsiveness such as metal ion/temperature and photothermal stimuli. For the first kind, Guo et al. used poly(N-isopropylacrylamide) (pNIPAM), a thermosensitive polymer that undergoes reversible gel to solution transition at 32℃. Combining with Ag+ triggered solution to gel transition, the DNA hydrogels undergo reversible transition across solution-gel-solid states [18]. Yata et al used AuNPs and AuNRs to produce thermo-responsive DNA hydrogels for photothermal cancer

immune therapy. Gold nanoparticles are modified with oligonucleotides and then mixed with hexapodnas DNA to form a hydrogel that will trigger immune responses in vivo upon laser irradiation at 532nm [19]. (Mention that in the second example, no polymer is in the hydrogel.)

Photo-responsive DNA hydrogels

Photo-responsive DNA hydrogels can be divided into two categories, one where the responsive group (nitrobenzyl or azobenzene) are located on the DNA strands, the other one is that the photosensitive components are the polymer. Kang et al. incorporated azobenzene into the backbone of the crosslinker DNA strand and polymerize in visible light to form a hydrogel. When the hydrogel was exposed to UV light, the azobenzene isomerizes from cis- state to trans-state and break the crosslinking. Another study used ethylene glycol diglycidyl ether (EDGE) to bind with G bases of the DNA to form a photosensitive hydrogel. The UV light will degrade the polymer, leading to a lower degree of crosslinking and larger mesh size and inducing the release of DNA and other molecules from the hydrogel network [20].

In this thesis, we utilized a nitrobenzyl derivative-modified ssDNA and copolymerized it with PEGDA to form a UV photo-responsive hydrogel that oligonucleotides segments can be cleaved under UV exposure and diffuse out of the gel.

1.3, Hydrogel fabrication
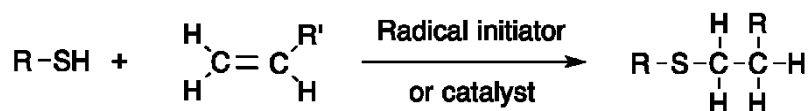
1.3.1, PEG and PEG derivatives

Polyethylene glycols (PEGs) are hydrophilic oligomers or polymers synthesized from ethylene oxide consisting of the repeat unit of $-(O-CH_2-CH_2)-$. Attaching a variety of reactive functional groups to the terminal sites of PEG polymers (hetero- or homo-bifunctional derivatives) can greatly expand their ability to crosslink agents, forming

hydrogel networks or act as spacers between two chemical entities [21]. PEG-based hydrogels have advantages over natural hydrogels, such as the ability for photopolymerization, tunable mechanical properties and easy control of scaffold structure and functionalization [22]. So, PEG hydrogels are excellent for tissue engineering and stimuli-responsive biomaterials. In this thesis, we utilized polyethylene glycol diacrylate (PEGDA) with a molecular weight of 575 for hydrogel fabrication.

1.3.2, Peptide-PEG conjugation

Though PEGs possess various advantages, they cannot provide us with an ideal environment to support cell adhesion and further applications due to their bio-inert nature. To improve the cell adhesion ability of PEG hydrogel, a frequently used method is to incorporate the cell adhesion peptide containing Arg-Gly-Asp (RGD) sequence into the network [23]. The most commonly used approaches to conjugate PEG molecules to peptides involve forming covalent bonds with (i) thiols in cysteine residues [24,25] or (ii) primary amines in lysine [26] residues or in the amino-terminal end of the molecule. In this thesis, we utilized a cysteine containing RGD peptides to directly react with acrylate group on PEGDA by thiol-ene reaction (a kind of click chemistry), and then the Acrylate-PEG-RGD and PEGDA will

$$R-SH \; + \; \underset{H}{\overset{H}{C}}=\underset{H}{\overset{R'}{C}} \; \xrightarrow[\text{or catalyst}]{\text{Radical initiator}} \; R-S-\underset{H}{\overset{H}{\underset{|}{C}}}-\underset{H}{\overset{R}{\underset{|}{C}}}-H$$

Basic schematic of thiol-ene addition reaction

polymerize and form a hydrogel. With this method, we can build stimuli-responsive co-DNA-PEG hydrogels that can response to input signals from cells.

1.3.2, Photo-initiators

In the photopolymerization process of hydrogels, photoinitiators are important for

absorbing irradiation and form free radicals to initiate chain propagation and crosslinking into a network. Generally, photoinitiators are classified into two categories, UV photoinitiators, and visible light initiators. UV light photoinitiators are the most commonly used initiators for hydrogel fabrication especially when the size or the resolution requirement of the gel is down to micron scale such as in 3D printing. Though UV photoinitiators such as Irgacure 2100 and Irgacure 2959 have very high efficiency and supports high precision polymerization, several drawbacks impede its versatile use in biomaterial or biomedical areas. For example, most UV initiators are cytotoxic. Also, the UV light will cause biomolecules denaturalization including DNA and proteins and UV have limited penetration depth [27]. Visible light initiators are widely used in dentistry for dental composite resins curing, some examples of vis-initiators including camphorquinone (blue light), phenylpropanedione, monoacrylphosphine oxide (TPO), bisacrylphosphine oxide, Irgacure 847 (green light) [28], eosin Y (green light) [29], riboflavin, tris(2,2-bipyridyl) dichlororuthenium(II) hexahydrate / sodium persulfate (abbreviation: Ru/SPS, wavelength 400-450nm)[30] and so on. Visible light initiators provide us with the possibility to integrate UV photosensitive reactions onto the hydrogel network. Here, the most commonly used camphorquinone/amine system will be highlighted in this section and its mechanism and kinetics will be briefly introduced.

In the CQ/amine system, the absorption of one quantum of radiation promotes the carbonyl group to an excited singlet. The excited singlet may also undergo intersystem crossing to the triplet state. Then the excited triplet (as the electron acceptor) forms an exciplex with the readily reduced amine (as the electron donor) by charge transfer from nitrogen lone pair to the carbonyl and thus producing two radical ions [31] and the polymerization rate is approximately

proportional to the square root of radiation intensity ($R_p \propto I_0^{1/2}$). It has been shown by Cook and Davidenko et al that amines with an abstractable proton on the -carbon undergo significant rates of polymerization and comparing the efficiency of different amine in enhancing initiation, they found that tertiary > secondary > primary amine [32,33]. They also demonstrate that for CQ concentrations of 0.05 -1.0 wt%, at low amine concentrations the polymerization rate grows and approach a peak value (≈0.6wt% of amine) and then at higher amine contents it decreases. The reason for this effect is that excess of amine will retard the polymerization in terms of a chain transfer process where the rate of the addition of amine radical to the monomer is slower than that of the chain propagation reaction. Therefore, in this thesis, we chose triethanolamine, a tertiary amine as the co-initiator at a concentration close to its maximum, 0.5 w/v %, and the concentration of CQ we chose was 0.8wt %.

1.4, Microfluidic devices

Microfluidics is the science of manipulating and controlling fluids, usually in the range of microliters (10^{-6}L) to picoliters (10^{-12}L), in networks of channels with dimensions from tens to hundreds of micrometers. The benefits of microfluidics include (i) reduced sample and reagent volumes, (ii) fast sample processing, (iii) high sensitivity, (iv) low cost, (v) portability, (vi) the potential to be highly integrated and automated that can prevent errors from manual manipulation. Based on these advantages, microfluidics is always considered as a platform for point of care biomedical and chemical applications, called lab-on-a-chip (LOC). For example, inertial microfluidic devices have been widely used in extraction of blood plasma, separation of particles and cells, solution exchange, isolation of target cell type, cell encapsulation, etc. [34] As a clinical diagnostics and detection platform, a variety of procedures can be arranged

side-by-side inside the device while the fluid flow throughout the chip. Yoav et al developed a valve-controlled LOC biosensor with ssDNA probes functionalized onto the patterned gold electrodes, such device allowed determination of DNA hybridization [35]. In recent years, with the development of bioprinting technology, microfluidic devices are used as a printing nozzle integrated within a custom 3D bioprinter that allows for the decomposition of multi materials in a single scaffold by rapidly switching between bio-inks or extruding multiple ingredients simultaneously [36,37]. Also, microfluidic systems are the most suitable platforms for research based on concentration gradient such as cell migration behaviors under diffusion controlled chemical gradient and DNA reaction-diffusion mechanisms [38,39]. In this work, we focused on the diffusion behavior of DNA molecules within PEGDA hydrogels. Therefore, we utilized microfluidic chips for two main benefits: precise hydrogel patterning with fixed height and a closed system with convenient solution switching function that suitable for diffusion.

1.5, Maskless photolithography: DMD

A digital micromirror device (DMD[TM], Texas Instrument) is a dynamic mask generator and is frequently used in 2D and 3D bioprinting with resolution requirement down to the micron scale. The mechanism of DMD is as follow, firstly, the desired pattern is designed into CAD model and then dynamically generates as a bitmap image on a programmable array of digital micro-mirrors on the DMD chip. The light illuminated on the chip is shaped into the pattern and transfer through the lens, thus, an image is formed on the hydrogel precursor solution [40].
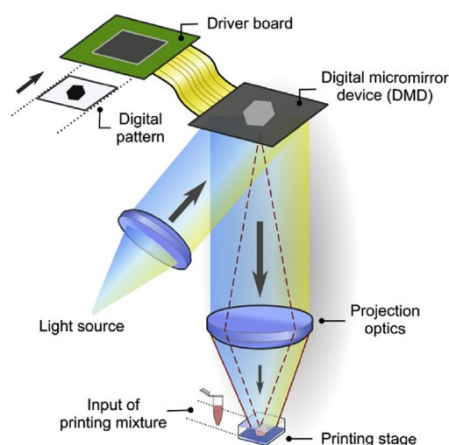
Diagram of DMD mechanism [30]

DMD is an excellent tool for cell-laden tissue construction because it allows fabrication of complex internal features along with precise spatial distribution of biological features in a single scaffold [41,42]. In this work, we used DMD to fabricate 2D patterned hydrogel in microfluidic channels.

1.6, The scope of my thesis

Emerging stimuli-responsive DNA biomaterials offer the possibility of integrating synthetic materials with biological molecules to regulate function and modulate biochemical signaling processes on a cellular level. Advances in fabrication techniques and the development of new biocompatible chemistries suggest new ways of tuning a material's responsiveness to different stimuli and broaden the applications of the materials. Digital maskless photolithographic patterning is becoming an increasingly powerful tool for the construction of two and three-dimensional soft biomaterials with specific architectures for applications such as lab-on-chip devices, engineering tissue scaffolds, drug delivery, and micromechanical and chemo-mechanical systems. Ultraviolet wavelength-absorbing photoinitiators are widely utilized in DNA-based hydrogel fabrication but have significant drawbacks, such as compatibility with biomolecules including DNA and crosstalk with many UV-photosensitive chemistries. In this thesis, we aimed at developing a method for the UV-photocleavable DNA-based hydrogel fabrication with digital maskless photolithography techniques. First, we optimized the formulation of camphorquinone, triethamolamine, and PEGDA (Mw = 575) suitable for the digital micro-mirror device to obtain well-patterned co-PEGDA-DNA hydrogels. Then, we demonstrated the control of UV-cleavage of acrylate modified DNA with a 1-(2-nitrophenyl) ethyl spacer to cleave DNA from selected regions.
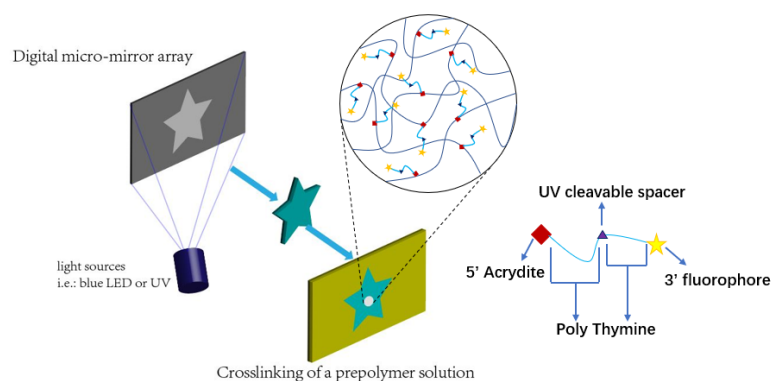
Diagram of UV photocleavable hydrogel fabrication

2, Methods and results

2.1, Hydrogel Fabrication

Our goal is to create a patterning method for hydrogels which satisfies the following three criteria:

i) The capability of integrating DNA into the hydrogel network.

ii) Enabling oligonucleotides diffusion (both inward and outward).

iii) The hydrogel is stiff enough to be isolated from microfluidic devices.

Our first step was to determine an optimal formulation for our hydrogel. To start with, a precursor mixture consists of 30v/v% PEGDA, 0.8w/v% CQ, 0.5v/v% TEA and 10v/v% 10x TAE Mg^{2+} buffer (Tris base, acetic acid, EDTA) is used and polymerized in a 100μm height microfluidic chip based on the formulation with another initiator - Irgacure 2959 (λ= 365nm). TAE buffer is needed for further experiments to ensure homogeneous mixtures of hybridized DNA. Optimal CQ and TEA concentrations were obtained from literature by Cook [39] and Jakubiak [40]. However, the efficiency of blue light (λ= 470nm) initiator CQ is lower than that of Irgacure 2959 and other UV photo-initiator [41], leading to a low polymerization rate and

much webbing around the desired pattern. Therefore, we increased the PEGDA percentage and adjusted the exposure time until it reached the ideal resolution. A formulation of 75v/v% PEGDA and 4sec exposure time produced gels with clear boundaries. However, the mesh size of our hydrogel will also decrease when increasing the monomer (PEGDA 575) content, which will impede oligonucleotides diffusion. In addition, we implemented a new setup to isolate the hydrogels from microfluidic devices, where we first cut the previous channel in half and anneal it with glass slide to make an open channel. The gels should be stiff enough to maintain its shape during the washing-out step.

With the optimal gel formulation, we successfully obtained patterned gels of high fidelity isolated from the microfluidic channels. Wide field images are showed in Figure 1. The small dots inside the hydrogel were the polystyrene particles (diameter = 5.11μm) we used for focusing.

However, when 1μM Cy3 fluorophore was added to the prepolymer solution, we observed phase separation phenomenon through Cy3 filter on the microscope, illustrating that prepolymer solution with high percentage as 75% PEGDA is heterogeneous. (In our first attempt of 30% PEGDA in the formulation with 1μM Cy3, we did not observe phase-separation phenomenon.)
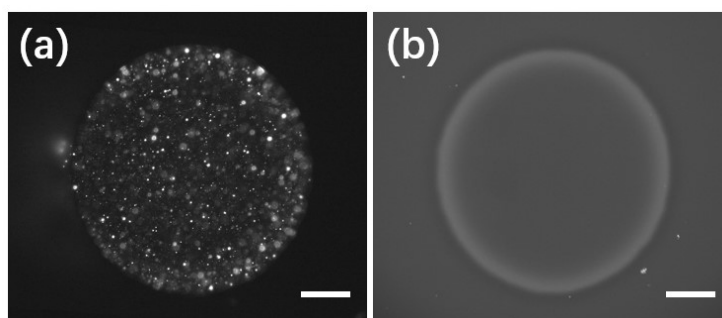

Figure 1. (a) Gel image of the phase-separation of 75% PEGDA with 1μM Cy3 (1xTAE Mg2+ buffer). (b) Homogeneous gel of 75%PEGDA with 1μM Cy3 (no buffer).
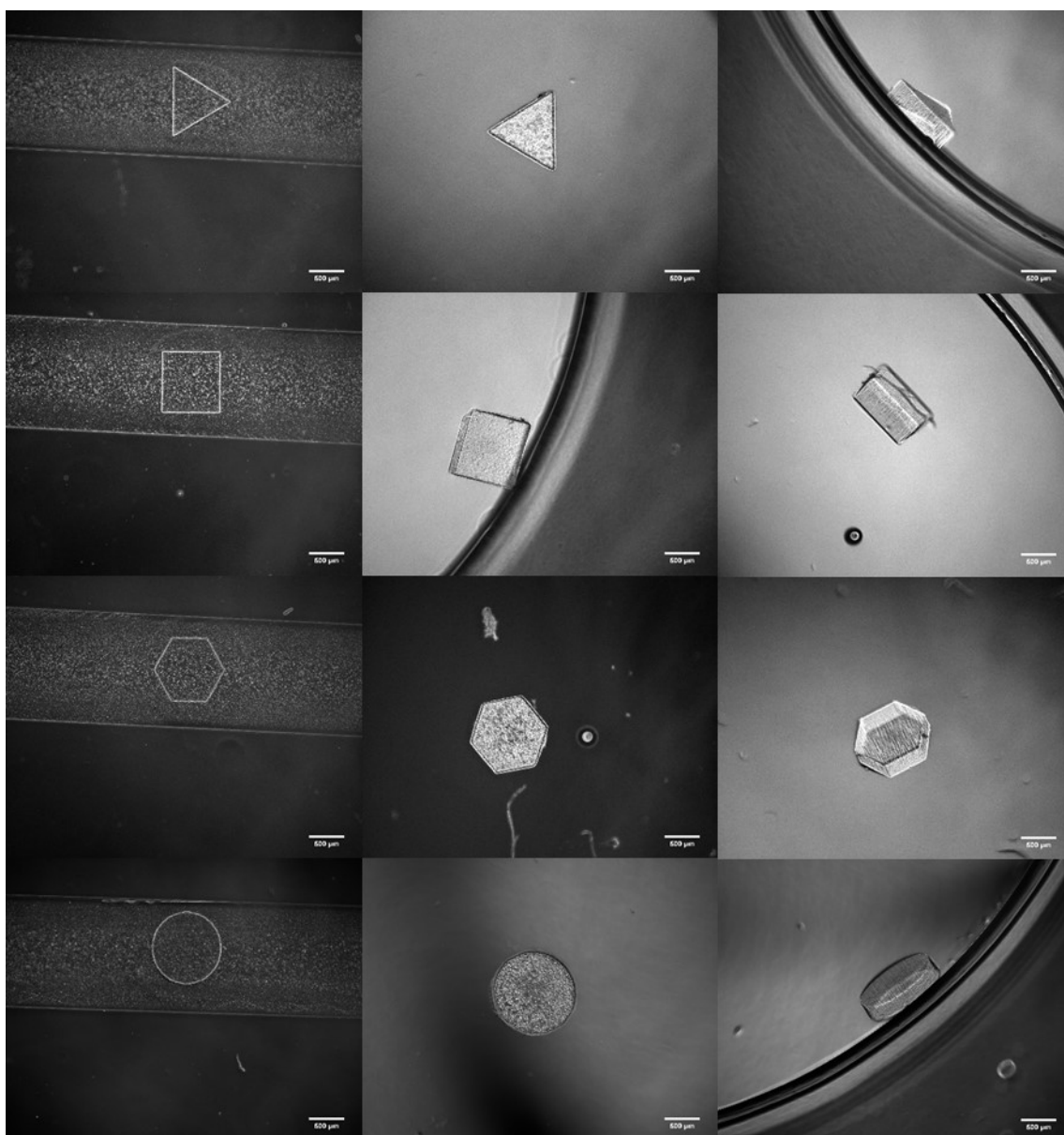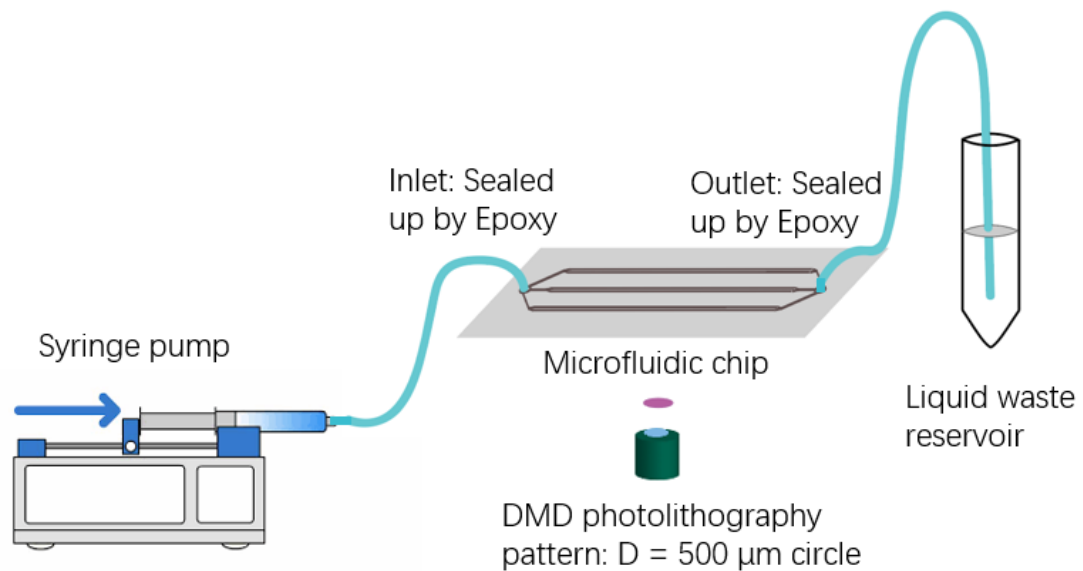
Figure 1. Gel patterns. The first column showed the patterned gels in the channel using DMD. The second column showed the top views of isolated gels in a 10mm diameter dish. The third column showed the side looks of gels in the dish. (Scale bar = 500μm)

Our theory was that the TAE buffer is the cause of phase-separation. To eliminate this effect, we reduced 10xTAE Mg^{2+} dosage by half (final buffer concentration is 0.5xTAE Mg^{2+}) in our prepolymer solution, sonicated for 10min and vortexed for 1min to make sure the prepolymer solution was well-mixed. Results showed that the phase-separation was reduced but still existed, which supported our theory. We next removed TAE Mg^{2+} from the formulation, and the effect was successfully eliminated. The effect of removing salt (Mg^{2+}) on double-

stranded DNA stability was not a concern because TAE Mg^{2+} buffer can be injected in the microfluidic devices and diffuse into the hydrogel afterward.

2.2, Measurements of DNA diffusion rates (with circular gels D=500um)

After proving that we have achieved ideal pattern-fidelity and stiffness of the assembled hydrogels, the next step was to test the rates of DNA diffusion inside the hydrogels. Diffusion was tested in two ways, outward and inward. Passive diffusion was carried out by polymerizing a gel with Cy3 modified DNA (5 base pairs and 31 base pairs in length), washing with 1xTAE Mg^{2+} to remove uncrosslinked prepolymer solution and then stopping the flow to see if the DNA can diffuse out. The inward diffusion was tested by polymerizing a 'blank gel', washing with 1xTAE Mg^{2+} and then injecting a DNA solution into a microfluidic chip containing the patterned hydrogel. The experimental setup is illustrated in as follows. Based on our experimental setup, diffusion was driven by the concentration gradient only.

Inlet: Sealed up by Epoxy   Outlet: Sealed up by Epoxy

Syringe pump

Microfluidic chip

Liquid waste reservoir

DMD photolithography pattern: D = 500 μm circle

Schematic of the experimental setup

2.2.1 Factors that affect the rate at which DNA molecules diffuse into the gel

2.2.1.1 Comparison of gel mesh size and DNA hydrodynamic radius

As I stated in the previous section, increasing the PEGDA 575 percentage will cause a decrease in hydrogel mesh size due to higher crosslinking density. To check the feasibility of DNA diffusion from the most straightforward manner is to compare the gel mesh size and the DNA hydrodynamic radius. If DNA hydrodynamic radius is larger than the mesh size, diffusion will not occur in our gel.
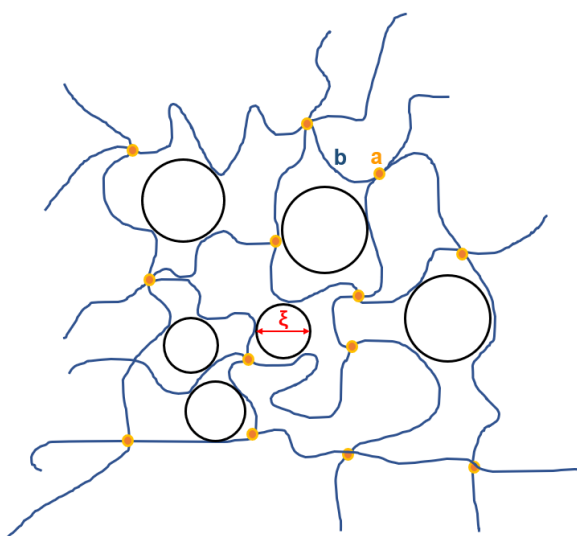
Schematic of the crosslinked structure of a hydrogel, indicating the crosslinks (a), the crosslinked chains (b), and the average mesh size ξ.

As demonstrated in the schematic above, when polymer chains are crosslinked in a thermodynamically good solvent, they attain a configuration of the solvated state. The characteristic correlation length, ξ, defines the average distance of the consecutive crosslinks and is also known as the mesh size in the theory of solute diffusion in polymers [42]. The equilibrium degree of swelling, q, is required to estimate the structural parameters such as molecular weight between crosslinks. However, at this stage, we didn't measure the actual swelling ratio, the value we used for calculation was based on literature and speculation. The polymer volume fraction before and after swelling is normally written as $v_{2,r}$, and $v_{2,s}$. In our

setup, $v_{2,r} = 0.75$. The polymer volume fraction after swelling was developed by Peppas[43,44] :

$$v_{2,s}^{-1} = q \cdot \frac{\rho_{PEGDA}}{\rho_{gel}} \tag{1}$$

Where ρ_{PEG} is the density of the PEGDA 575 (1.12 g/cm^3), ρ_{gel} is the density of the hydrogel (assume to be 1 g/cm^3). Based on the observation of our experiment, the swelling ratio of our gel was small. Therefore, I postulate the value range to be [2, 2.5]. Then $v_{2,s}$ has the range of [0.357, 0.446].

Then we calculated the number average molecular weight between crosslinks [6]:

$$\frac{1}{\bar{M}_c} = \frac{2}{\bar{M}_n} - \frac{\left(\frac{\bar{v}}{V_1}\right)\left[\ln(1 - v_{2,s}) + v_{2,s} + \chi v_{2,s}^2\right]}{v_{2,r}\left[\left(\frac{v_{2,s}}{v_{2,r}}\right)^{1/3} - \frac{v_{2,s}}{2v_{2,r}}\right]} \tag{2}$$

Here, $\bar{v}$ is the specific volume of amorphous PEGDA (0.892 mL/g), V_1 is the molar volume of water (18.1 mL/mol), χ (0.426) is the PEGDA-water Flory-Huggins interaction parameter which can be found in tables.

Mesh size was then determined by Canal and Peppas [43]. The root-mean-square end to end distance of the polymer chain can be calculated by the following equation:

$$\left(\bar{r}_o^2\right)^{1/2} = l \cdot C_n^{1/2} \cdot n^{1/2} \tag{3}$$

Where l is the average bond length of one repeat unit, in our case is 0.297 nm (the sum of C-C bond, 0.154nm, and C-O bond, 0.143nm), C$_n$ is the characteristic ratio of the polymer (here we used the value for PEG 6.9 as estimation), and n is the number of bonds in the crosslink:

$$n = 2 \cdot \frac{\bar{M}_c}{M_r} \tag{4}$$

Where M_r is the molecular weight of the repeat unit (44 for PEGDA). Mesh size was then be calculated by the following equation:

$$\xi = v_{2,s}^{-1/3} \cdot \left(\overline{r_o}^2\right)^{1/2} \qquad [5]$$

The mesh size of our gel according to our assumption should be in the range of [3.52nm, 5.17nm].

The next step was to estimate the size of DNA molecules where we consider DNA hydrodynamic diameter as the main parameter. When nucleic acids are dissolved in solutions, their chains will coil and form a structure that we assume to be a sphere, also, nucleic acids are highly hydrated and at least the first hydration shell of the water moves hydrodynamically with the macromolecule [45]. The hydrodynamic radius R is often called the Stokes radius and can be related to other molecular parameters. Generally, a polymer with molecular weight M and partial specific volume $\bar{v}_2$ has minimum molecular volume and radius $V_{min} = \frac{M\bar{v}_2}{N_A} = \frac{4}{3}\pi R_{min}^3$, where N_A is Avogadro's number so the minimum radius is

$$R_{min} = \left(\frac{3M\bar{v}_2}{4\pi N_A}\right)^{1/3} \qquad [6]$$

If we replace $\bar{v}_2$ with the hydrated specific volume, $\bar{v}_2 + \delta_1 v_1^0$, based on the assumption that δ_1 grams of water (specific volume v_1^0) are associated with 1g of dry polymer, the hydrated radius can be calculated by the following equation:

$$R_0 = R_{min}\left(1 + \frac{\delta_1 v_1^0}{\bar{v}_2}\right) \qquad [7]$$

For nucleic acids, $\delta_1 = 0.5$g/g, $v_1^0 = 1.0$cm^3/g, and $\bar{v}_2 = 0.56$ cm^3/g, the ratio was found to be $R_0/R_{min} = 1.24$.

In our experiment, we used two single strand DNA. The molecular weight of the two strands is 1520 g/mol for polyT5 and 9345.63g/mol for 31 bases strand. The diameters of the molecules are 1.726nm and 3.16nm.

The calculation showed that the diameter of DNA is slightly smaller than the mesh size. Therefore, it is expected that diffusion can occur in our hydrogel.

2.2.1.2, Calculating DNA diffusion constants using Fick's law of diffusion

To quantify the DNA diffusion rate within our hydrogels, we need to build a model based on the accurate description of our experimental conditions. A circular gel is simple enough to fabricate as well as to obtain an analytical solution for data fitting. By assuming the gel is radially uniform, we can create a 2-D cylindrical model with two variables, r, and θ, where r is the distance of an arbitrary position from the center, θ is the angle of the position with respect to a starting radius. Therefore, the temporal concentration inside the gel is a function of spatial variable r and time variable t, that is, C(r, t). Here, the spatial dependence of concentration has been simplified to a 1D system where θ is not taken into consideration due to the radial homogeneous attribute. In a cylindrical coordinate system, the Fick's second law of diffusion has the following form:

$$\frac{\partial C}{\partial t} = D \frac{1}{r} \frac{\partial}{\partial r} \left(r \frac{\partial c}{\partial r} \right) \qquad [8]$$

Based on our experiment setup, taking passive diffusion as an example, the gels were polymerized in the microfluidic channel with 1uM Cy3 modified DNA in the prepolymer solution, and then we pumped in the buffer to wash out the pre-gel solution and surround the gel with buffer and start image, recording t = 0. Under this circumstance, the initial and boundary conditions are:

I.C.: $C(r, t = 0) = 1, r < R;$ $\qquad$ $C(r, t = 0) = 0, r \geq R.$

B.C: $C(r = R, t) = 0;$ $\qquad$ $\frac{\partial C(r=0,t)}{\partial r} = 0.$

The first step to seek for a solution is to separate the variables. We postulate a solution

that is the product of two functions, T(t), a function of time only and P(r), a function of radial

coordinate r only. With this assumption, the solution can be written as:

$$C(r, t) = P(r) \cdot T(t) \tag{9}$$

Substituting equation [2] for C in diffusion equation [1], we can obtain:

Left hand side:

$$\frac{\partial C}{\partial t} = \frac{\partial [P(r) \cdot T(t)]}{\partial t} = P(r) \cdot \frac{\partial T(t)}{\partial t} \tag{10}$$

Right hand side:

$$D \frac{1}{r} \frac{\partial}{\partial r} \left(r \frac{\partial c}{\partial r} \right) = D \frac{1}{r} \frac{\partial}{\partial r} \left(r \frac{\partial [P(r) \cdot T(t)]}{\partial r} \right) = D \cdot T(t) \frac{1}{r} \frac{\partial}{\partial r} \left(r \frac{\partial P(r)}{\partial r} \right) \tag{11}$$

Equation [10] equals [11], divide the both sides by D•P(r)T(t), we can obtain the

following result:

$$\frac{1}{D} \frac{1}{T(t)} \frac{\partial T(t)}{\partial t} = \frac{1}{P(r)} \frac{1}{r} \frac{\partial}{\partial r} \left(r \frac{\partial P(r)}{\partial r} \right) = -\lambda^2 \tag{12}$$

The LHS is a function of t only and the RHS is a function of r only, therefore the only

way this can be right is both sides equal a constant, which we assign it to be $-\lambda^2$.

The general solution for $\frac{\partial T(t)}{\partial t} = -\lambda^2 D T(t)$ is $T(t) = A e^{-\lambda^2 D t}$.

The RHS equation can be written as: $r^2 \frac{\partial P(r)^2}{\partial^2 r} + r \frac{\partial P(r)}{\partial r} + \lambda^2 r^2 P(r) = 0$. The general

solution to this equation is $P(r) = B J_0(\lambda r) + C Y_0(\lambda r)$, where J_0 and Y_0 are the Bessel

Functions of the first and second kind with zero order. Thus, the general solution for

concentration becomes:

$$C(r, t) = P(r) \cdot T(t) = A e^{-\lambda^2 D t} [B J_0(\lambda r) + C Y_0(\lambda r)] = e^{-\lambda^2 D t} [C_1 J_0(\lambda r) + C_2 Y_0(\lambda r)] \tag{13}$$

In our case, at any time t, $\lim_{r \to 0} C(r, t) = finite$, whereas $\lim_{r \to 0} Y_0(\lambda r) = -\infty$, therefore

$C_2=0$. Apply boundary condition $C(r = R, t) = 0$, we get following equation:

$$e^{-\lambda^2 D t} [C_1 J_0(\lambda R)] = 0 \tag{14}$$

20

The solution for $J_0(\lambda R) = 0$ can be found in tables that give the zero points for Bessel functions. We use symbol α_{m0} to indicate the mth zero point of J$_0$, with $\lambda_m R = \alpha_{m0}$, we can get a complete set of solution for equation [14]:

$$C(r, t) = \sum_{m=1}^{\infty} C_m\, e^{-\lambda_m^2 Dt} J_0(\lambda_m r) \qquad [15]$$

Apply the initial condition $C(r, t = 0) = 1$:

$$C(r, 0) = 1 = \sum_{m=1}^{\infty} C_m J_0(\lambda_m r) \qquad [16]$$

The constants value Cm can be found from the general equation of orthogonal eigenfunction expansions including the weighting function equaling to r.

$$C_m = \frac{\int_0^R r J_0(\lambda_m r)\, dr}{\int_0^R r [J_0(\lambda_m r)]^2\, dr} = \frac{\frac{R J_1(\lambda_m R)}{\lambda_m}}{\frac{R^2}{2}[J_1(\lambda_m r)]^2} = \frac{2}{\lambda_m R J_1(\lambda_m R)} = \frac{2}{\alpha_{m0} J_1(\alpha_{m0})} \qquad [17]$$

Put [17] into equation [15], and substitute $\frac{\alpha_{m0}}{R}$ for λ_m, the final solution for passive diffusion equation is obtained:

$$C(r, t) = \sum_{m=1}^{\infty} \frac{2}{\alpha_{m0} J_1(\alpha_{m0})} e^{-\alpha_{m0}^2 \frac{Dt}{R^2}} J_0\left(\alpha_{m0}\frac{r}{R}\right) \qquad [18]$$

In a similar way, the inward diffusion equation has a solution as:

$$C(r, t) = 1 - \sum_{m=1}^{\infty} \frac{2}{\alpha_{m0} J_1(\alpha_{m0})} e^{-\alpha_{m0}^2 \frac{Dt}{R^2}} J_0\left(\alpha_{m0}\frac{r}{R}\right) \qquad [19]$$

Equation [11] and [12] are the diffusion data fitting models in the following sections.

2.2.2, Single-stranded DNA diffusion

2.2.2.1, Passive diffusion of PolyT5

The experiment was implemented as illustrated in the schematic in section 2.2, and 1μM of Poly T5 was mixed in the pregel solution for photopolymerization and image every 3

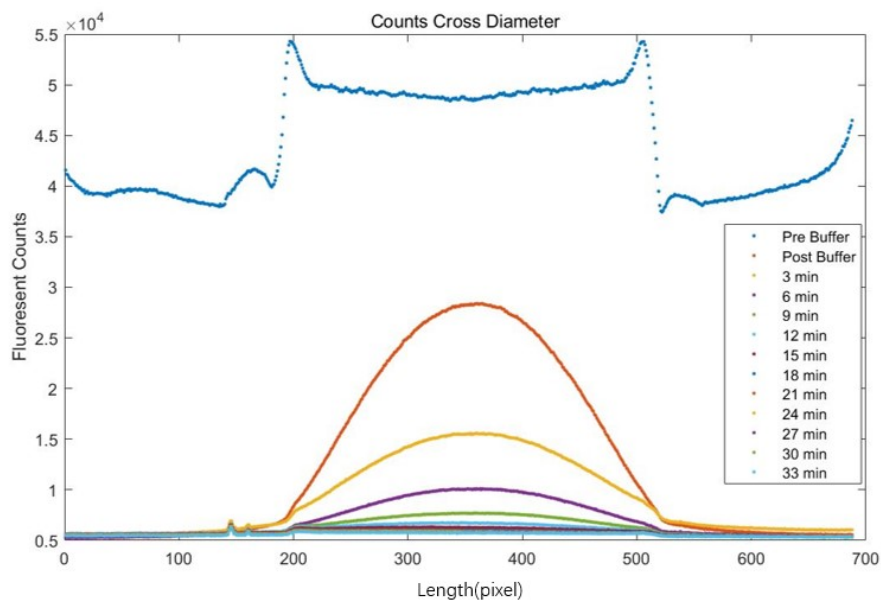minutes to capture the diffusion profile (Figure 2).

Figure 3. Diffusion profile across the diameter

Figure 3 showed the fluorescent count of the gel and the surrounding solution. After about 33 minutes, polyT5 molecules fully diffused out of the hydrogel. The first time point illustrates that right after polymerization, there is a strange effect inside the gel leading to higher counts inside than that of the surrounding solution. Our conjecture was that the optical property of the hydrogel is different from pregel solution. However, our main purpose focused on the diffusion, the optical effect wasn't our concern.
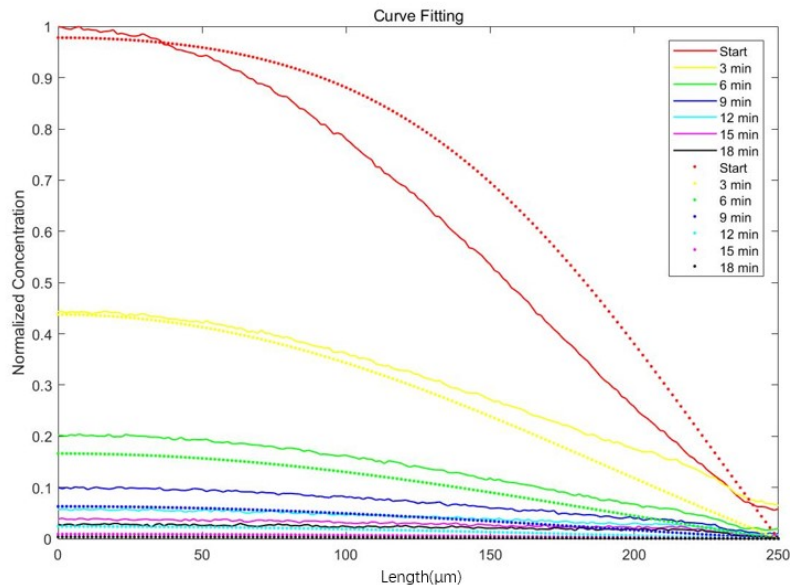
Figure 4. Normalized data fitting for polyT5

Fitting the data to the model we built in section 2.2.1.2 using a least square curve fit to a single variable, diffusion coefficient D, which gave us a result with standard deviation of D = 41.828 $\pm$ 3.7896 μm^2/s for polyT5 within 75% PEGDA, 0.8% Camphorquinone, 0.5% TEA at a radiant exposure of 45.6 mJ/cm^2 from a blue LED light guide intensity of 11.4 mW/cm^2 for an exposure of 4 seconds.

2.2.2.2, Passive diffusion of 31 bases ssDNA

The same setup was implemented to measure the diffusion constant of a 31 base ssDNA molecule. Different dosages of blue light were used during patterning to get a better understanding of how the rates at which DNA molecules diffuse into hydrogels as a function of hydrogel density. 1μM of DNA was mixed in pregel solution and exposed using blue LED for 1 second (11.4 mJ/cm^2), 2 seconds (22.8 mJ/cm^2), 3 seconds (34.2 mJ/cm^2), and 4 seconds (45.6 mJ/cm^2). The first image was taken right after photopolymerization, rest of images were taken immediately after buffer injection and repeatedly every 5 minutes.
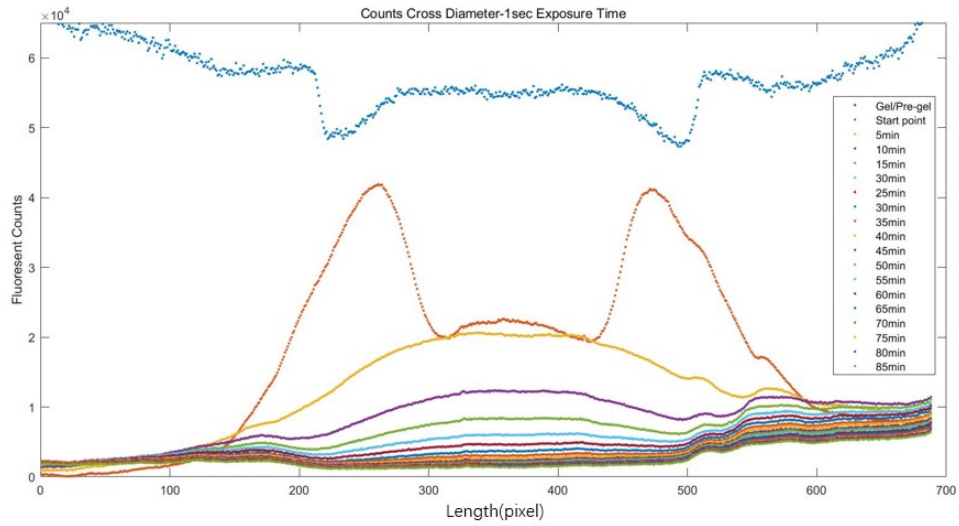
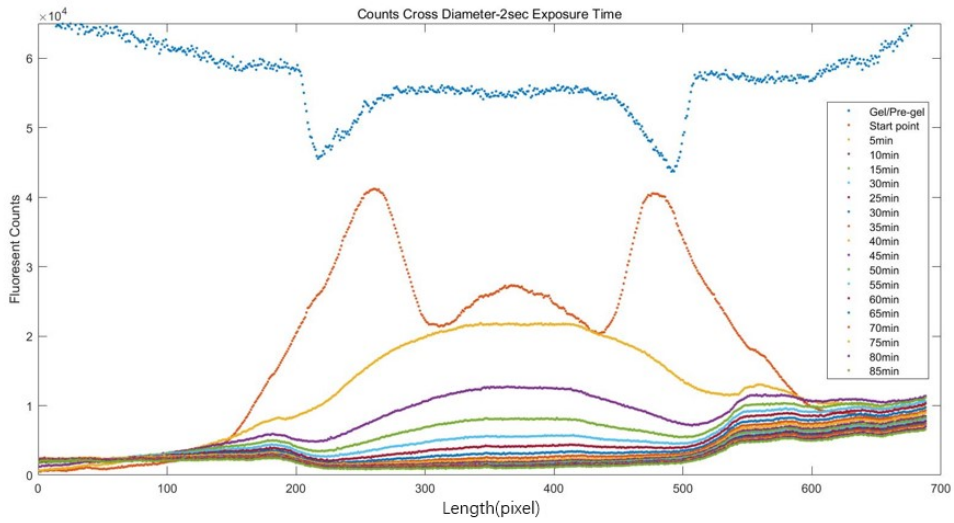Figure 5. Diffusion profile across the diameter for 1 second-exposure gel

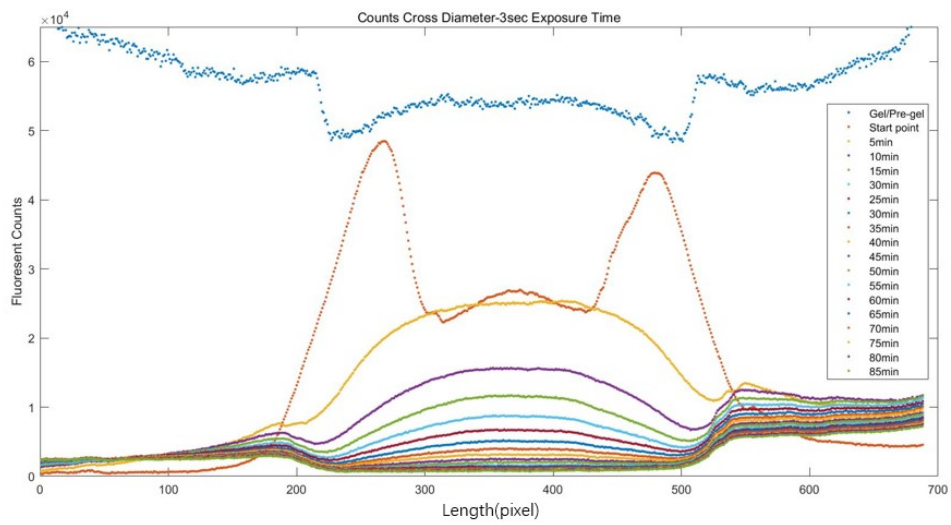Figure 6.Diffusion profile across the diameter for 2 second-exposure gel

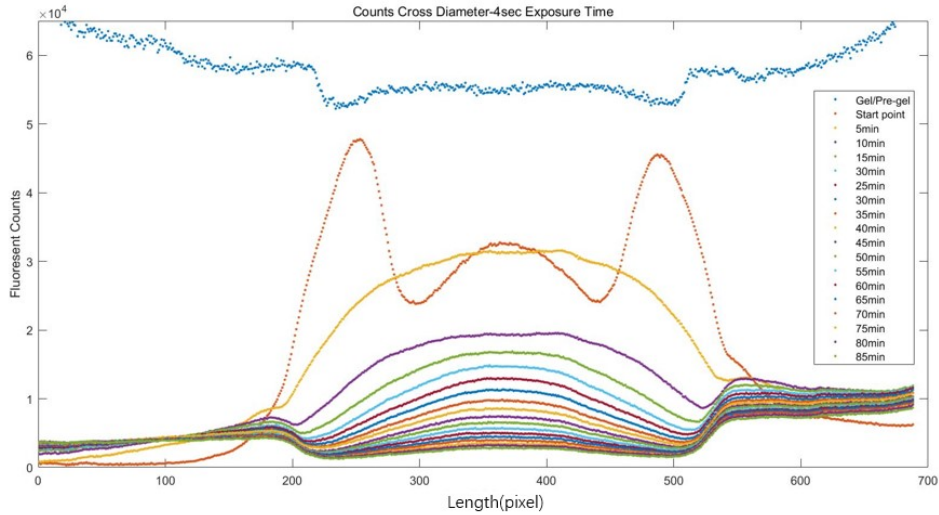Figure 7. Diffusion profile across the diameter for 3 second-exposure gel

Figure 8. Diffusion profile across the diameter for 4 second-exposure gel

Comparing Figure 5-8, we can find out that increasing the exposure time of polymerization, the diffusion rate decreased, which is reasonable. As I mentioned in section 1.3.2, the level of excited photo-initiator is relevant to the radiant dosage, the longer the exposure time, the more camphorquinone molecules were excited, and the higher density of crosslinking, leading to a smaller mesh size which will retard diffusion.

Similarly, strange effects were also observed after polymerization and buffer injection, also at the gel boundaries. Those effects will impede us from obtaining accurate diffusion coefficients in the data fitting process. Therefore, the inward diffusion experiment described in the next section was used to measure diffusion rates.

2.2.2.3, Diffusion of 31 base single strand DNA

The same DNA strand was used as in section 2.2.2.1. Prepolymer solution with no test DNA was injected and photo-polymerized for 1 second, 2 seconds, 3 seconds or 4 seconds. The excess prepolymer was washed by the 1xTAE buffer, and then 1uM of 31 bases ssDNA was injected to the device and imaged every 5 minutes.

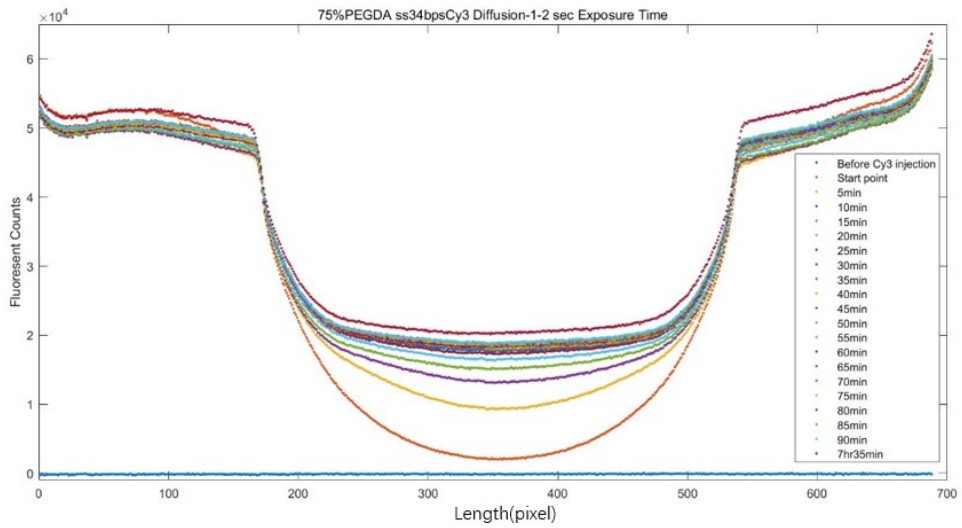•Plotting the fluorescent counts cross the diameter:

Figure 9. Diffusion profile across the diameter for 1 second-exposure gel
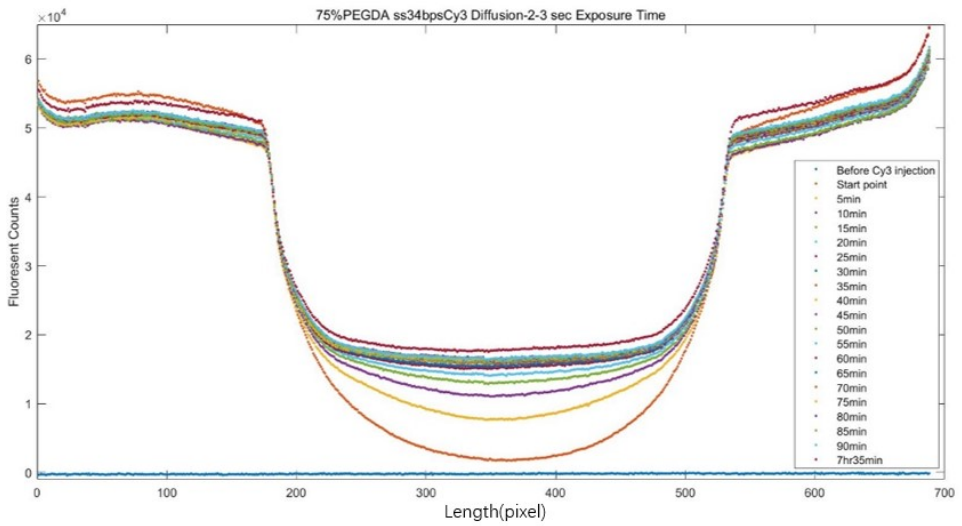

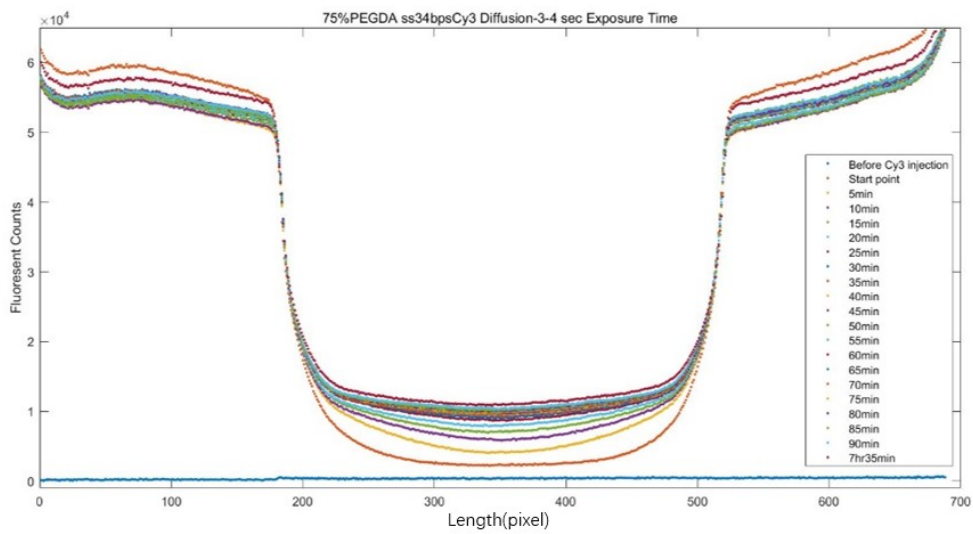Figure 10. Diffusion profile across the diameter for 2-second-exposure gel

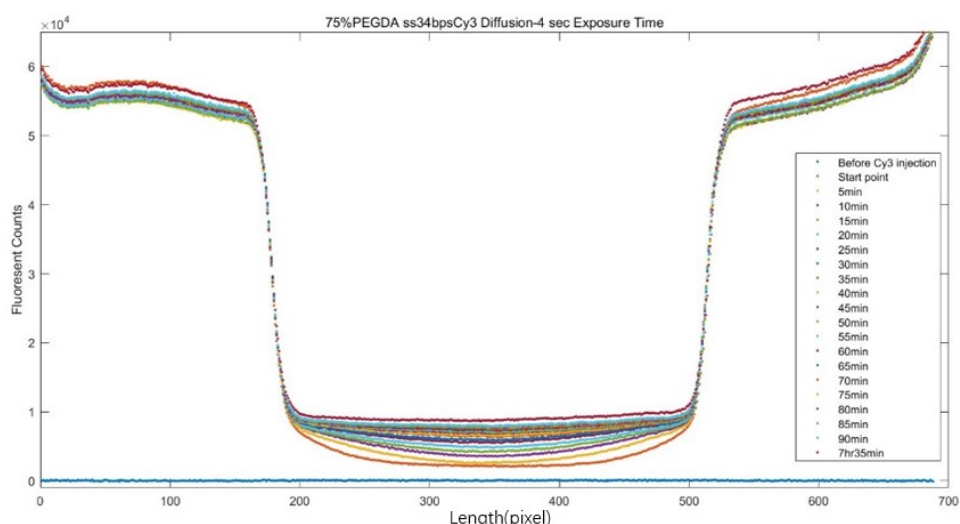Figure 11. Diffusion profile across the diameter for 3-second-exposure gel

Figure 12. Diffusion profile across the diameter for 4-second-exposure gel

At equilibrium, large offsets between equilibrium fluorescent count inside the gel and in surrounding solution. Amsden explained solute behavior in hydrogels in terms of reduction in hydrogel free volume, enhanced hydrodynamic drag on the solute, longer path length due to obstruction and a combination of both hydrodynamic drags and obstruction. The last two theories explain the reason for the retarded solute diffusion rate within hydrogels comparing within the liquid phase [46]. Free volume theory describes solute diffusion as jumping into voids formed in the solvent space, where the voids are pictured to be formed by a general withdrawal of liquid molecules due to thermal motion and then the voids are filled in by solute molecules. The available free volume for solute diffusion inside the gel including the redistribution of water molecules and the redistribution of polymer molecules, whose contribution is tiny, and the polymers can be considered as immobile network inside the hydrogel. Therefore, the volume accessible for solutes are the voids between the polymer chains. There are several definitions used for solute concentration within the gels, including solute per unit volume of gel (denoted C_G), the amount of solute per unit void volume (denoted C_V), and the amount of solute per unit gel volume at the equilibrium (denoted C_E). For porous media like hydrogel,

$C_G = (1 - \varphi) \cdot C_V$ is always satisfied, where φ stands for the polymer volume fraction. To describe the relationship between C_E and C_G, Muhr et al.[47] introduce partition coefficient K defined by $C_G = KC_E$. In most cases, the solutes won't be adsorbed by polymer chains, the prediction of K is the geometric exclusion effect that the fractional volume for large solute molecules (denoted $1 - \Phi$) is less than that of smaller molecules (denoted $1 - \varphi$), meaning that smaller molecules can reach close to the void boundaries. Thus, for smaller molecules $K = 1 - \varphi$, while for larger solutes $K = 1 - \Phi$. In our cases, the dimension of DNA molecules is close to the mesh size of the hydrogel (calculated in section 2.3.1.1), which means the available fractional volume for DNA was small and caused the offset. Also, increasing exposure time lead to smaller mesh size and larger Φ, resulting in a decrease in the equilibrium concentration.

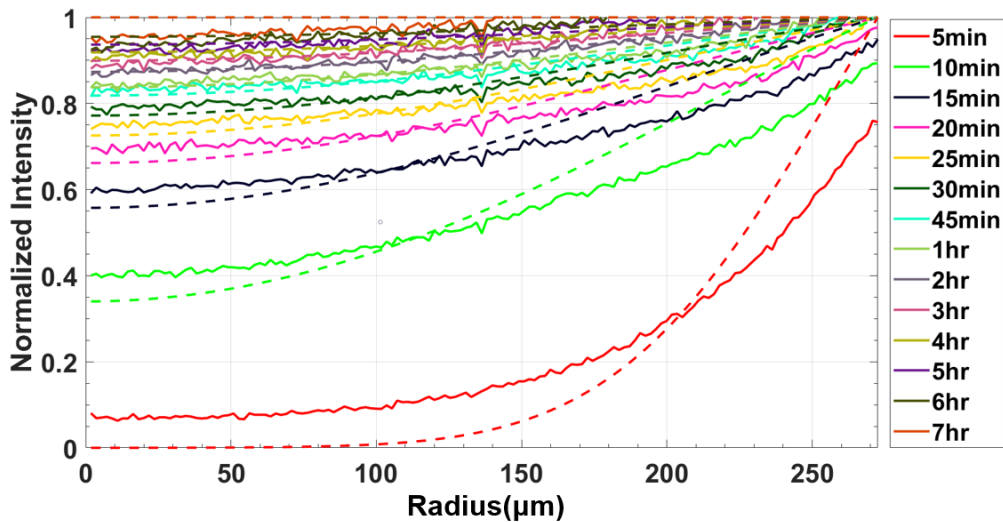We took $C_E = 1\ \mu M$, and fit the data to the model (Equation [19]):

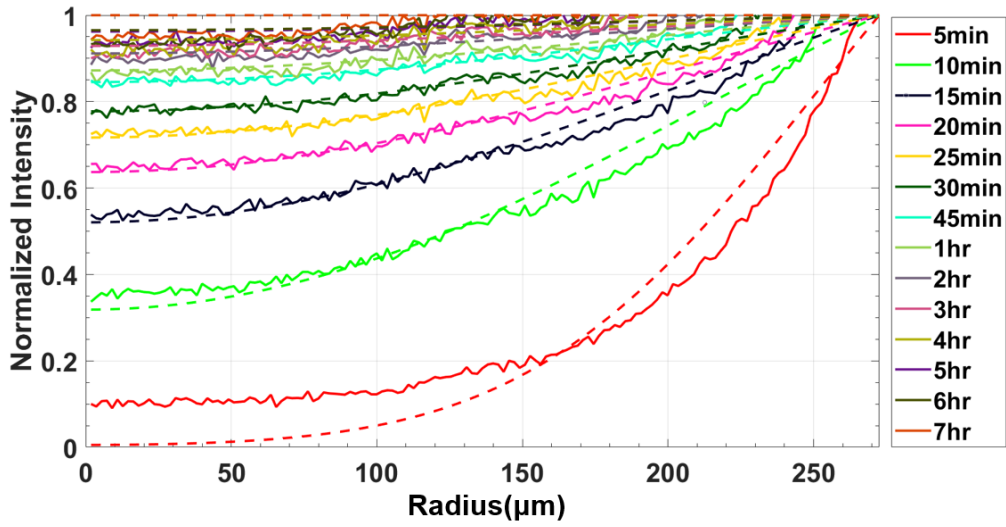Figure 13. Normalized data fitting for 1-sec-exposure gel

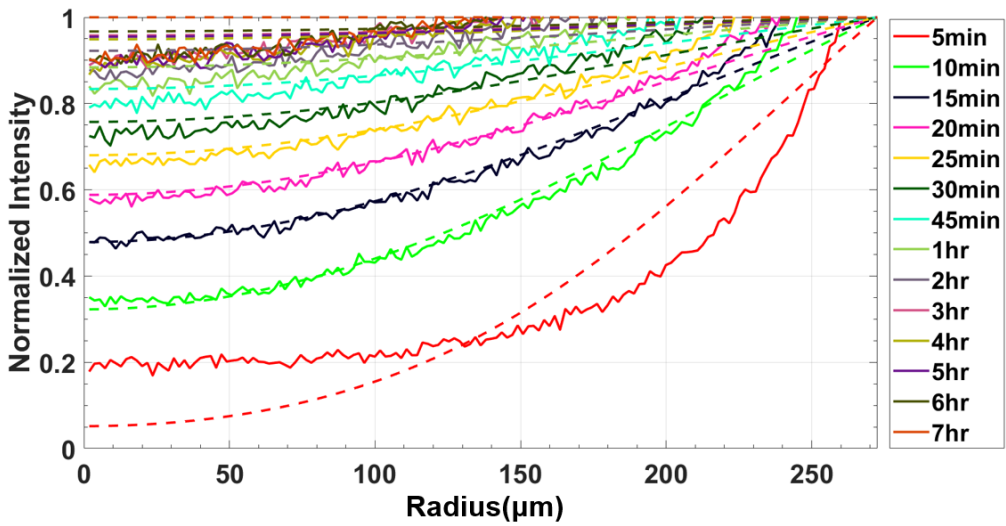Figure 14. Normalized data fitting for 2-sec-exposure gel

Figure 15. Normalized data fitting for 3-sec-exposure gel
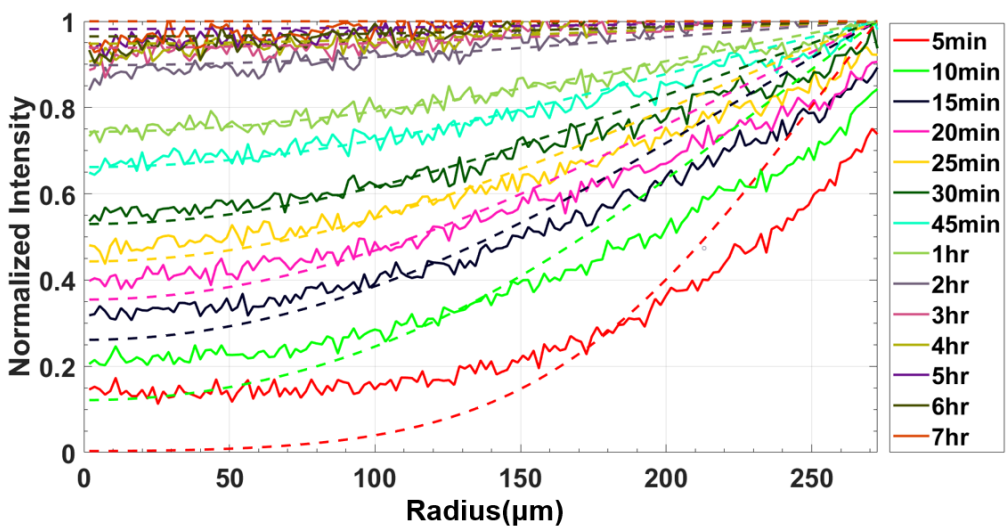
Figure 16. Normalized data fitting for 4-sec-exposure gel

Figure 12-15 gave us diffusion coefficients with stand deviations of 16.0075 $\pm$

$5.88\mu m^2/s$, $17.9953 \pm 6.9591\mu m^2/s$, $14.8833 \pm 5.6579\mu m^2/s$, and $10.4274 \pm 5.1823\mu m^2/s$ for 1 second (11.4 mJ/cm^2), 2 seconds (22.8 mJ/cm^2), 3 seconds (34.2 mJ/cm^2), and 4 seconds (45.6 mJ/cm^2) exposure.

2.2.3, Double-stranded DNA diffusion

Double-stranded DNA was made by hybridizing 31 base DNA (same strand used in 2.3.2.2) with R4 anchor strand. Diffusion experiment for dsDNA was carried out with the same setup, but injecting 500nM of DNA.
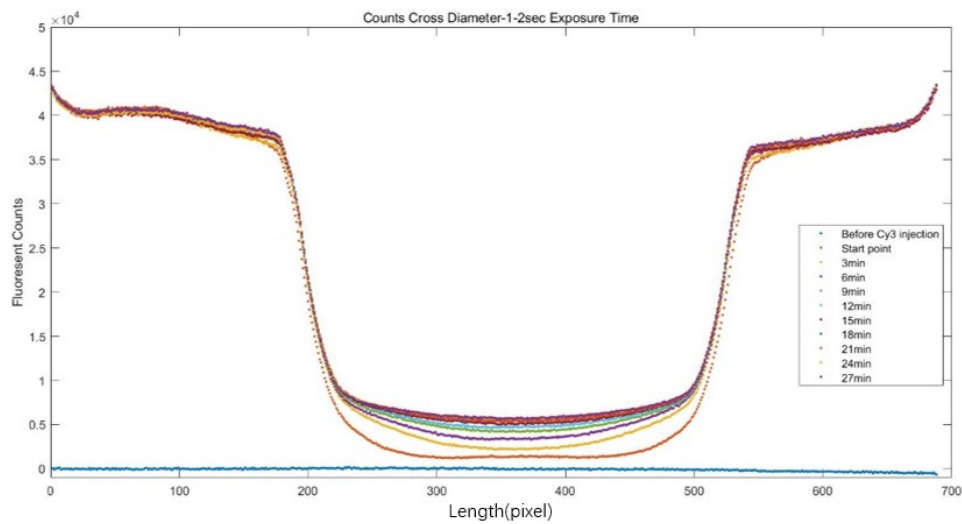
Figure 17. Diffusion profile across the diameter for 1-second-exposure gel
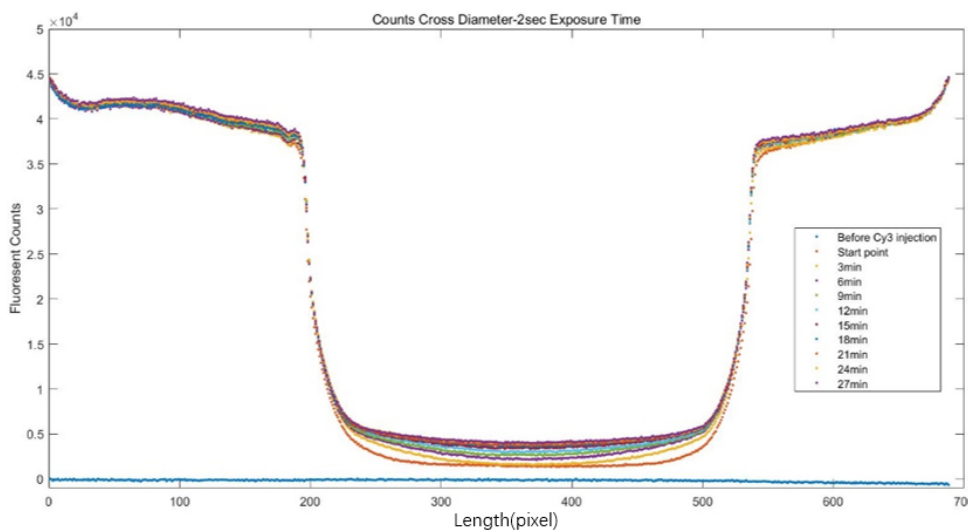
Figure 18. Diffusion profile across the diameter for 2-second-exposure gel
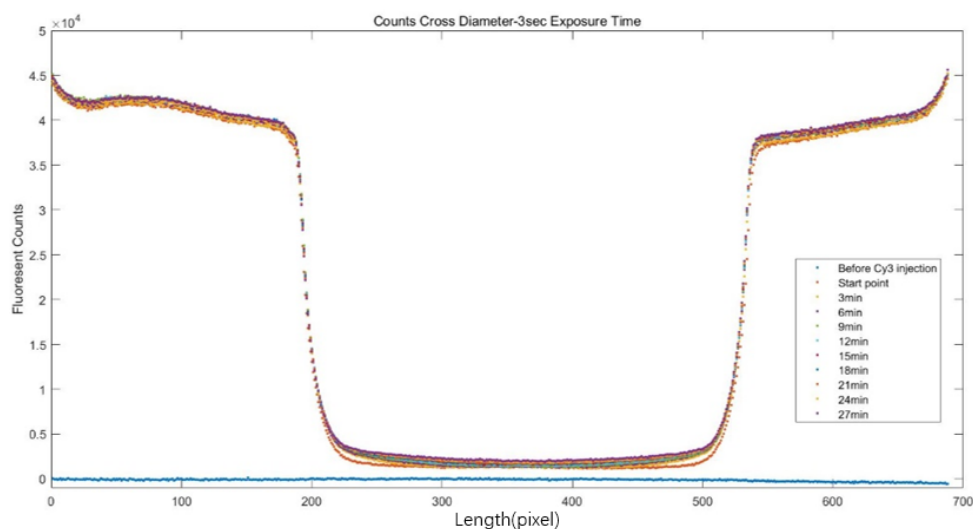
Figure 19. Diffusion profile across the diameter for 3-second-exposure gel
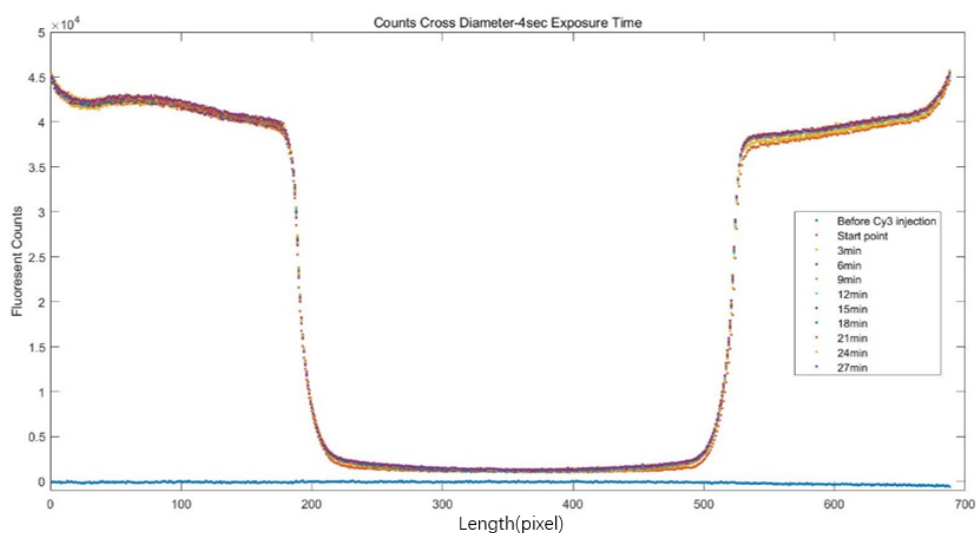
Figure 20. Diffusion profile across the diameter for 4-second-exposure gel

2.3, DNA acrydite retention

DNA retention was quantified by mixing 2μM acrydite-modified Cy3 labeled fluorescent DNA strand in the prepolymer solution and photopolymerizing to integrate DNA onto the hydrogel network. The fluorescent count level was obtained after washing by 20mL 1xTAE Mg^{2+} using a syringe pump programmed at a flow rate of 1mL/hr. Assuming that the concentrations have a linear correlation with Cy3 fluorescence with the camera setting we used, we can normalize the data by the following equation:

$$Normalized\ counts = \frac{Raw\ image - dark\ image}{Raw\ image(t=0) - dark\ image}$$

Where $Raw\ image$ is the raw data of average fluorescence within the gel, $dark\ image$ is the average fluorescent counts of the surrounding solution, and $Raw\ image(t=0)$ is the initial fluorescent level before wash. Standard deviation was calculated from 3 replicates.
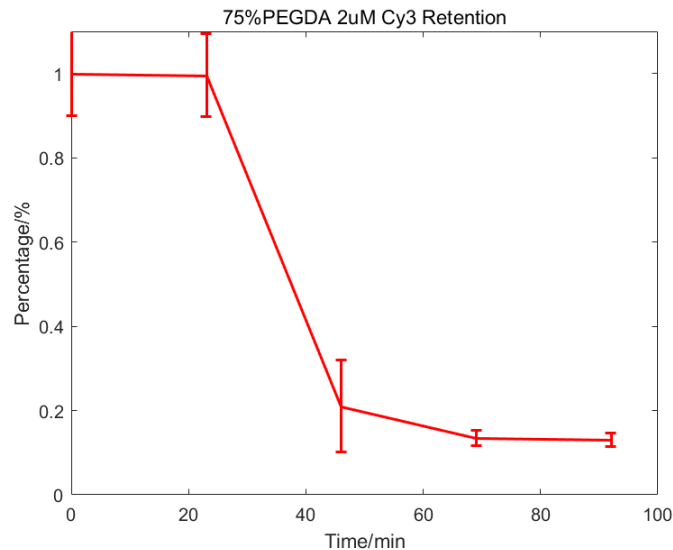
Figure 21. DNA acrydite retention

For the given formulation of 75% PEGDA, 0.8% camphorquinone, 1% TEA, and 4-second exposure at 11.4 mW/cm^2 from blue LED, Figure 20 showed the percentage of DNA anchored is about 12%, which is very low compared with other photoinitiators such as Irgacure 2100 which can give us a DNA retention percentage about 55%, indicating the low efficiency of camphorquinone.

2.4, Measurements of DNA UV photo-cleavage

We identified Cyanine 3 as a DNA dye modification that exhibited minimal photobleaching when exposed to UV-A light. To verify our consideration, solutions of Cyanine 3 labeled DNA was exposed to UV-A light emitted from a UVP transilluminator for 2 hours. We observed a 4.25% average change in the fluorescent level of the solution over that period.

To check whether camphorquinone potentially degraded Cy3 dye fluorescence activity during excitation under UV light, we also exposed solutions of Cyanine 3 labeled DNA mixed with 0.8 % (w/v) CQ for 2 hours and observed an average reduction in fluorescence intensity of 35.4% (Figure 21). Based on the 'bleach' effect of CQ on Cy3-labeled DNA, we washed 75% (v/v) PEDGA hydrogels containing crosslinked Cy3-labeled DNA with butanol for more than 10 hours to remove residual camphorquinone. We performed control UV exposure experiments where we polymerized co-PEGDA-DNA hydrogels at 470 nm light containing acrydite polyT10-Cy3 oligonucleotide with no photocleavable spacer and camphorquinone/triethanolamine; after performing a butanol wash, the gels were exposed to a 200 μm diameter circular pattern UV light (Dosage = 180 J cm^{-2}). An average intensity change of 0.015 is observed in the exposed regions of the gel which is small enough to be ignored. It is important to note that it was not the aim of this work to identify DNA fluorophore modifications that are compatible with CQ, this examination was to determine a protocol to obliviate the degradation as much as possible and obtain more accurate results.
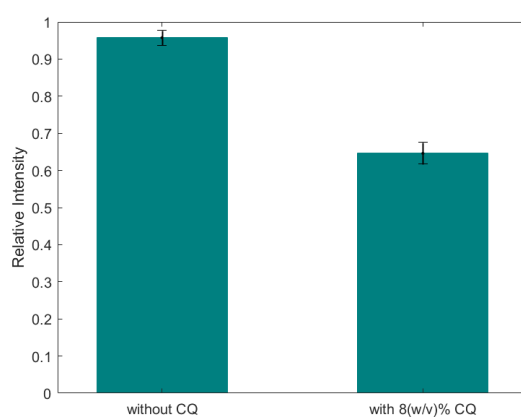
Figure 22.Relative intensity after UV-A exposure

To determine the efficiency of UV-triggered photo-cleavage by cleaving a 1-(2-nitrophenyl)ethyl spacer in the backbone of anchored fluorophore-modified oligonucleotides,

we first crosslinked of 5' acrydite-polyT10 DNA (2 μM concentration in the prepolymer) within 400 μM diameter circles inside the branched flow cell using a 75%(v/v) PEGDA formulation exposed to 470 nm light (dosage = 57 mJ cm^{-2}) and wash with water overnight letting uncrosslinked DNA to diffuse out. The polyT10 strand contained an internal UV-photocleavable spacer inserted in the middle of the 10 bases, and a 3' Cy3 dye modification. We exposed UV light in a 200 μM diameter circle pattern onto each hydrogel. To estimate the efficiency of the UV-triggered photocleavage process as a function of energy dosage, different sets of hydrogels within the flow cell were exposed for dosages of 45 J cm^{-2}, 90 J cm^{-2}, and 135 J cm^{-2} (intensity = 25 mW cm^{-2} at 365 nm).

Figure 23. The average center intensity of hydrogels after UV exposure as a function of UV dosage (average ± s.d.).
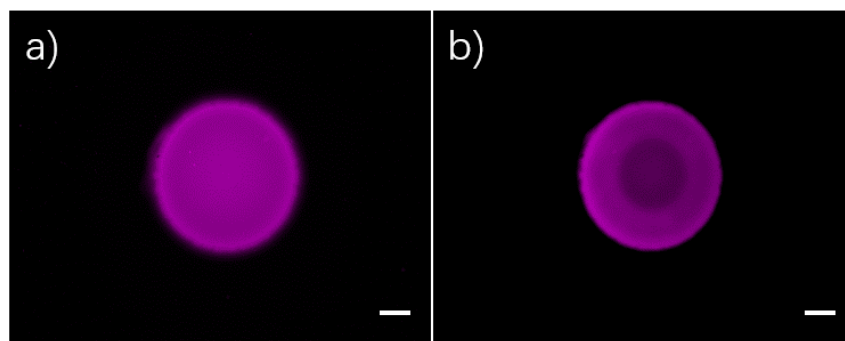
Figure 24. Prior and after exposure. Patterned 75% (v/v) co-PEGDA-Cy3 DNA hydrogel prior to (a) UV exposure and after exposure (b) to a 200 μm diameter UV pattern, dosage = 1350 J cm^{-2} (scale bars = 100 μm).

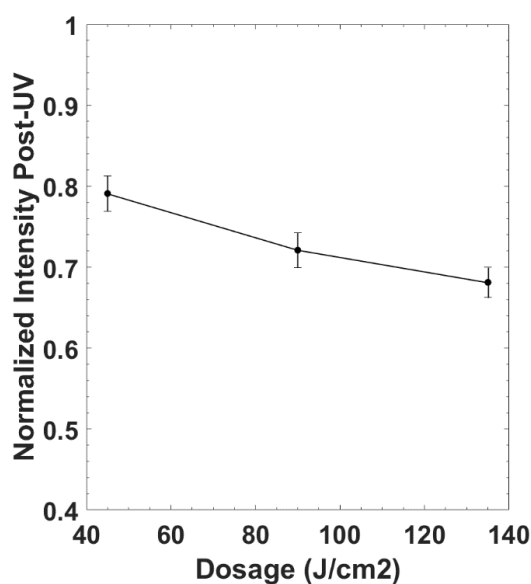Fluorescent images of the 75% (v/v) co-PEGDA-DNA hydrogels after UV exposure showed decreased fluorescent intensity in the exposed regions (Figure 23 a-b). The average normalized intensities in the center of the hydrogels immediately after exposure to the UV light were 0.80 ± 0.01, 0.72 ± 0.01, and 0.68 ± 0.01, corresponding to UV dosages of 45 (30min), 90 (1 hr), and 135 J cm^{-2} (1.5hr) (Figure 22). Reduction in the relative intensity in UV exposed areas indicated that fluorescence decrease resulted from the photocleavage of 1-(2-nitrophenyl) ethyl linker, as well as the diffusion of the fluorophore fragments from out of the gel. We have stated that the average intensity change of 0.015 in co-PEGDA-DNA hydrogel containing acrydite polyT10-Cy3 DNA with no photocleavable spacer can be neglected. We attribute the decrease in intensity due to cleavage and diffusion of the fluorophore from the center of the gel and not due to changes in gel structure or photo-induced degradation of Cy3 dye.

2.5, Cell culture on PEGDA gel

Inspired by the co-DNA-PEGDA hydrogel force sensor work in our lab, we hope that we can detect and even measure cell adhesion force exerted on the gel surface. In this section, we tried a cyclo RGD peptide containing Cystine that can react bind to
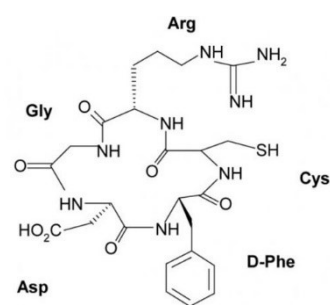
Structure of cycloRGD

acrylate ends on PEGDA through thiol-ene reaction to support cell adhesion. The hydrogel formulation was obtained from our group member working on force sensor project. Here, we used the formulation of 20v/v% PEGDA, 0.5v/v% Irgacure 2100, 10v/v% 10x TAE Mg^{2+}, 5mM cycloRGD (cycloRGD was pretreated by TCEP for thiol deprotection). Prepolymer solution was added into a PDMS mold to make hydrogel square sheet (0.5mm x 0.5mm x 600 μm), polymerized on a UV transilluminator at 365nm for 30min (dosage of 450 J/cm^2). Hydrogels were soaked into MilliQ water for 24 hours to remove residual reagents, and then we seeded HeLa cells (green fluorophore protein (GFP) labeled) in the 48 well plates.
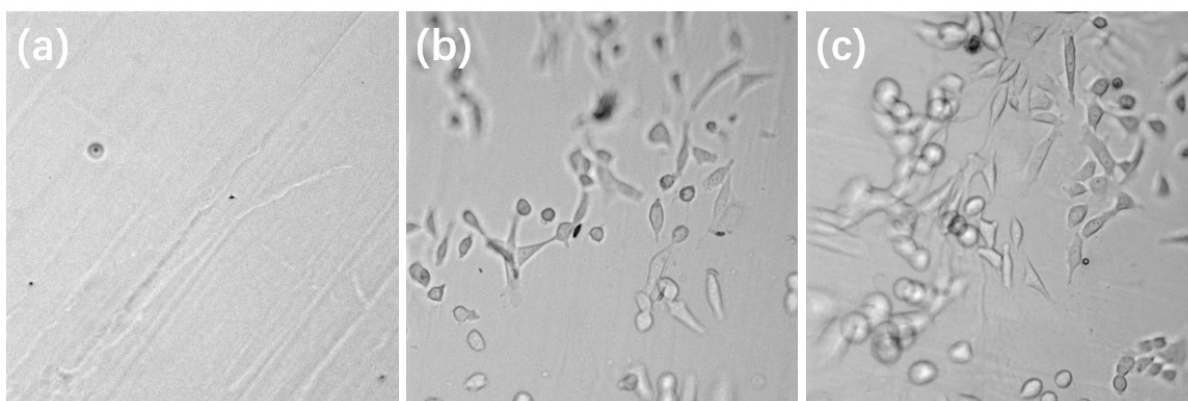
Figure 25. (a) Control group after 12 hours culture. (b) Cell culture after 12 hours on RGD-PEGDA hydrogel. (c) Cell culture after 36 hours on RGD-PEGDA hydrogel.

From the image, we found that after 12 hours of culture, HeLa cells adhered to the RGD-PEGDA hydrogel surface and proliferated in the following 24 hours, indicating that our method can successfully conjugate RGD with PEGDA and improve cell adhesion.

3, Conclusion and future perspective

The ability to photo-pattern hydrogels with a visible light initiator gives rise to a new category of smart materials. In this work, we first demonstrated that the co-PEGDA-DNA

hydrogel formulations composed of blue LED initiator system, camphorquinone and triethanolamine allows high-resolution patterned hydrogel fabrication with the help of digital maskless photolithography. Then we showed that we are able to trigger DNA photocleavage reaction in the UV exposed pattern. The technique provides us with the opportunity to assemble structurally complex stimuli-responsive DNA-based hydrogel that won't crosstalk with UV-sensitive photolabile chemistries. Furthermore, with our method, microgels are no longer restricted within the microfluidics device, leading to more freedom of utilization. However, there is still room for improvement in our work, for example, we have found that the polymerization efficiency of camphorquinone and triethanolamine was pretty low which will cause a waste of DNA and an excessive need of PEGDA in order to obtain the desired pattern. Future works will focus on finding more efficient visible light photoinitiators for the system. Such a platform may promote studies in pattern sensing and transmitting algorithms and UV triggered spatial programmable DNA reaction cascades.

References

Bibliography

[1] Kahn JS; Hu Y; Willmer I. Stimuli-Responsive DNA-Based Hydrogels: From Basic Principles to Applications. Accounts of Chemical Research. 2017,50,680-690.

[2] Qian L; Winfree E. Scaling Up Digital Circuit Computation with DNA Strand Displacement Cascades.Science. Vol.332, 2011,6,1196-1201.

[3] Orbach, R.; Willner, B.; Willner, I. Catalytic Nucleic Acids (DNAzymes) as Functional Units for Logic Gates and Computing Circuits: From Basic Principles to Practical Applications. Chemical Communications. 2015, 51, 4144−4160.

[4] Shahbazi MA; Ramos TB; Santos HA. DNA Hydrogel Assemblies: Bridging Synthesis Principles to Biomedical Applications. Advanced Therapeutics. 2018,1,1800042.

[5] Soto, A. M.; Loo, J.; Marky, L. A. Energetic Contributions for the Formation of TAT/TAT, TAT/CGC+, and CGC+/CGC+ Base Triplet Stacks. American Chemistry Society. 2002, 124, 14355 -14363.

[6] Davis, J. T.; Spada, G. P. Supramolecular Architectures Generatedby Self-Assembly of Guanosine Derivatives. Chem. Soc. Rev. 2007, 36,296−313.

[7] Xu L; Wang R; Kelso LC; Ying Y; Li Y. A target-responsive and size-dependent hydrogel aptasensor embedded with QD fluorescent reporters for rapid detection of avian influenza virus H5N1. Sensors and Actuators B. 234(2016) 98-108.

[8] Song P; Ye D; Zuo X; Li J; Wang J; Liu H; Hwang MT; Chao J; Su S; Wang L; Wang L;

Huang W; Lal Ratnesh; Fan C. DNA Hydrogel with Aptamer-Toehold-Based Recognition, Cloaking, and Decloaking of Circulating Tumor Cells for Live Cell Analysis. ACS NanoLetter. 2017 ,17 ,5193 -5198.

[9] Travascio P; Li Y; Sen D. DNA-enhanced peroxidase activity of a DNA aptamer-hemin complex. Chemistry & Biology. 1998 Sep;5(9):505-17.

[10] Huang Y; Xu W; Liu G; Tian L. A pure DNA hydrogel with stable catalytic ability produced by one-step rolling circle amplification. Chemical Communication. 2017, 53,3038.

[11] Um SH; Lee JB; Park N; Kwon SY; Umbach CC; Luo D. Enzyme-catalyzed assembly of DNA hydrogel. Nature Materials. 5, 797-801 (2006).

[12] Noll T; Reeb SW; Schonherr H; Noll G. Pristine DNA hydrogels from biotechnology derived plasmid DNA. Angewandte Chemie International Edition. 2017, 56, 12004-12008.

[13] Pang Q; Zheng X; Luo Y; Ma L; Gao C. A photo-cleavable polyprodrug-loaded wound dressing with UV-responsive antibacterial property. Journal Material Chemistry B. 2017, 5, 8975.

[14] Kim SM; Diamond SL. Photocleavage of o-nitrobenzyl ether derivatives for rapid biomedical release applications. Bioorganic & Medicinal Chemistry Letters. 16(2006) 4007-4010.

[15] MacCulloch T; Buchberger A; Stephanopoulos N. Emerging applications of peptide-oligonucleotide conjugates: bioactive scaffolds, self-assembling systems, and hybrid nanomaterials. Organic & Biomolecular Chemistry. 2019,17,1668.

[16] Guo W; Lu C; Orbach R; Wang F; Qi X; Cecconello A; Seliktar D; Willner I. pH-Stimulated DNA Hydrogels Exhibiting Shape-Memory Properties. Advanced Materials. 2014,27,73.

[17] Wilson WD; Gough AN; Doyle JJ; Davidson MW. Coralyne Intercalation with DNA as a possible mechanism of antileukemic action. Journal of Medicinal Chemistry. 1976,19 1261.

[18] Guo, W; Lu, CH; Qi, XJ; Orbach, R; Fadeev, M; Yang, HH; Willner, I. Switchable Bifunctional Stimuli-Triggered Poly-NIsopropylacrylamide/DNA Hydrogels. Angewandte Chemie International Edition. 2014, 53,10134−10138.

[19] Yata T; Takahashi Y; Tan M; Nakatsuji H; Ohtsuki Shiozo; Murakami T; Imahori H; Umeki Y; Shiomi T; Takakura Y; Nishikawa M. DNA nanotechnology-based composite-type gold nanoparticleimmunostimulatory DNA hydrogel for tumor photothermal immunotherapy. Biomaterials 146 (2017) 136-145.

[20] Staples CA; Boatman RJ; Cano ML. Ethylene glycol ethers: an environmental risk assessment. Chemosphere. 1998 Mar, 36(7): 1585-613.

[21] Hutanu D; Frishberg MD; Guo L; Darie CC. Recent Applications of Polyethylene Glycols (PEGs) and PEG Derivatives. Modern Chemistry & Applications. 2014,2:2.

[22] Zhu J. Bioactive modification of poly(ethylene glycol) hydrogels for tissue engineering. Biomaterials 31 (2010) 4639-4656.

[23] Yang F; Williams CG; Wang D; Lee H; Manson PN; Elisseeff J. The effect of incorporating RGD adhesive peptide in polyethylene glycol diacrylate hydrogel on osteogenesis of bone marrow stromal cells. Biomaterials 26 (2005) 5991–5998.

[24] Zhang C; Hekmatfer S; Karuri NW. 2014. A comparative study of polyethylene glycol

hydrogels derivatized with the RGD peptide and the cell-binding domain of fibronectin. J Biomed Mater Res Part A 2014:102A:170–179.

[25] Miller JS; Shen CJ; Legant WR; Baranski JD; Blakely BL; Chen CS. Bioactive hydrogels made from step-growth derived PEG–peptide macromers. Biomaterials 31 (2010) 3736–3743.

[25] Zhang J; Yan S; Yuan D; Alici G; Nguyen NT; Warkiani ME; Li W. Fundamentals and applications of inertial microfluidics: a review. Lab on a Chip. 2016,16,10.

[26] Yoav HB; Dykstra PH; Bentley WE; Ghodssi R. A controlled microfluidic electrochemical lab-on-a-chip for label-free diffusion-restricted DNA hybridization analysis. Biosensors and Bioelectronics. 64 (2015) 579–585.

[27] Colosi C; Costantini M; Barbetta A; Dentini M. Microfluidic bioprinting of heterogeneous 3D tissue constructs. Zuzana Koledova (ed.), 3D Cell Culture: Methods and Protocols, Methods in Molecular Biology, vol. 1612.

[28] Colosi; Shin SR; Manoharan V; Massa S; Costantini M; Barbetta A; Dokmeci MR; Dentini M; Khademhosseini A. Microfluidic bioprinting of heterogeneous 3D tissue constructs using low-viscosity bioink. Advanced Material. 2016,28,677-684.

[29] Murugesan N; Singha S; Panda T; Das SK. A diffusion based long-range and steady chemical gradient generator on a microfluidic device for studying bacterial chemotaxis. Journal of Micromechanics and Microengineering. 26 (2016) 035011.

[30] Wang X; Liu Z; Pang Y. Concentration gradient generation methods based on microfluidic systems. RSC Advances. 2017,7,29966.

[31] Sun C; Fang N; Wu DM; Zhang X. Projection micro-stereolithography using digital

micro-mirror dynamic mask. Sensors and Actuators A. 121 (2005) 113-120.

[32] Lu Y; Mapili G; Suhali G; Chen S; Roy K. A digital micro-mirror device-based system for the microfabrication of complex, spatially patterned tissue engineering scaffolds. Journal of Biomedical Material Research 77A. 396,2006.

[33] Grogan SP; Chung PH; Soman P; Chen P; Lotz MK; Chen S; D'Lima DD. Digital micromirror device projection printing system for meniscus tissue engineering. Acta Biomaterialia 9 (2013) 7218–7226.

[34] Ma X; Yu C; Wang P; Xu W; Wan X; Lai CSE; Liu J; Maharajh AK; Chen S. Rapid 3D bioprinting of decellularized extracellular matrix with regionally varied mechanical properties and biomimetic microarchitecture. Biomaterials 185 (2018) 310–321.

[35] Lim KS; Schon BS; Mekheleri NV; Brown GCJ; Chia CM; Prabakar S; Hooper GJ; Woodfield TBF. New visible-light photoinitiating system for improved print fidelity in gelatin-based bioinks. ACS Biomaterials Science and Engineering. 2016,2, 1752-1762.

[36] Arikawa H; Takahashi H; Kanie T; Ban S. Effect of various visible light photoinitiators on the polymerization and color of light-activated resins. Dental Materials Journal 2009; 28(4): 454–460

[37] Cruise GM; Hegre OD; Scharp DS; Hubbell JA. A sensitivity study of the key parameters in the interfacial photopolymerization of poly(ethylene glycol) diacrylate upon porcine islets.

[38] Cook WD. Photopolymerization kinetics of dimethacrylates using the camphorquinone/amine initiator system. Polymer, 1992, Vol 33, No 3.

[39] Davidenko N; Garcia O; Sastre R. Photopolymerization Kinetics of Dimethacrylate-

Based Light-Cured Dental Resins. Journal of Applied Polymer Science, Vol. 97, 1016–1023 (2005).

[40] Jakubiak,J; Wrzyszczynski, A; A Linden,L; Rabek, J.F. The Role of Amines in the Camphorquinone Photoinitiated Polymerization of Multifunctional Monomer. Journal of Macromolecular Science, Part A: Pure and Applied Chemistry, 2007,44:239-242.

[41] Arikawa, H; Takahashi, H; Kanie, T; Ban, S. Effect of various visible light photoinitiators on the polymerization and color of light-activated resins. Dental Materials Journal 2009,28(4): 454-460.

[42] Canal,T; Peppas N.A. Correlation between mesh size and equilibrium degree of swelling of polymeric networks. Journal of Biomedical Materials Research, Vol.23, 1183-1193 (1989).

[43] Hickey,A.S; Peppas,N.A. Mesh size and diffusive characteristics of semicrystalline poly(vinyl alcohol) membranes prepared by freezing/thawing techniques. Journal of Membrane Science, 107(1995)229-237.

[44] Zustiak,S.P; Leach, J.B. Hydrolytically degradable poly(ethylene glycol) hydrogel scaffolds with tunable degradation and mechanical properties. Biomacromolecules. 2010 May 10; 11(5): 1348-1357.

[45] Bloomfield VA; Crothers DM; Tinoco IJ. Nucleic acids: structures, properties and functions. Sausalito: University Science Books, 2000.

[46] Amsden, B. Solute diffusion within hydrogels. Mechanisms and models. Macromolecules, 1998, 31, 8382-8395.

[47] Muhr, A.H.; Blanshard, J.M.V. Diffusion in gels. Polymer, 1982, Vol 23, July.

Appendices: DNA Sequences

[1] 31 bases single-stranded oligonucleotides: CATCT CATAA CACAT CTCAC AATCC

ATCTC A

[2] Photocleavable DNA: 5' Acrydite-TTTTT/PC spacer/TTTTT-3'Cy3

Curriculum Vitae

Wenlu Wang

Home Address:
Room 3-1-1001, No.500 Gaoerji Road, Shahekou District, Dalian, Liaoning, China
Current Address:
500 University Pkwy, Apt 16 E, Baltimore, Maryland, United States (Available before 2019/6/11)
Zip code: MD 21210
Contact Information:
Mobile: +1 443 627 0455
Email: wwang102@jhu.edu or wenluwang950623@gmail.com

RESEARCH INTERESTS:

My current research centers around utilizing maskless photolithography (DMD) to fabricate hydrogels in microfluidic channels and triggering DNA diffusion-reaction in the hydrogel. I am interested in what I'm working on now and I'm also very interested in the functionalities of biomolecules (especially DNA and proteins) and stimuli-responsive biomaterials and their further applications in the field of medicine and healthcare.

EDUCATION

09/2013-07/2017
BACHELOR OF ENGINEERING
Sichuan University, Chengdu, China
•**Major: Light Chemical Engineering (Leather Chemistry and engineering)**
•**GPA: 3.46/4.00 (Ranking 5%)**
•**Core courses:** Principle of Chemical Engineering, Analytical Chemistry Experiment, Chemical Experiment, Basis of Modern Chemistry, Tanning Chemistry, Leather Chemicals
•**Title and Awards:**
Merit-based First-class Scholarships for consecutive two academic years, Outstanding

Student Cadre, University-Level Merit Student

09/2017-07/2019
MASTER OF SCIENCE AND ENGINEERING
Johns Hopkins University, Maryland, United Sates
•**Major: Chemical & Biomolecular Engineering**
•**GPA: 3.8/4.00**
•**Core courses:** Advanced Thermodynamics in Practice, Interfacial Nano Systems, Transport Phenomena in Practice, Advance Chemical Reaction Engineering, Metabolic Systems Biotechnology, Polymer Physics

RESEARCH EXPERIENCE

04/2015-04/2017
STUDENT RESEARCH TRAINING PROGRAM
Dr. Wei Lin's Lab, Sichuan University
•Project leader of ***Design, Preparation and Characterization of Composite Hydrogel Based on Modified Gelatin Nanoparticles***
Our goal is to introduce the natural macromolecule, gelatin, into polyacrylamide hydrogel to increase its biocompatibility and mechanical property. I modified gelatin with methacrylic anhydride and utilized this modified gelatin as a crosslinker and APS/TEMED as initiator and catalyst to obtain a gelatin-acrylamide composite hydrogel.

10/2017-03/2019
GRADUATE RESEARCH
Dr. Rebecca Schulman's Lab, Johns Hopkins University
•***A Digital Photolithographic Patterning Method for Poly (Ethylene Glycol) Diacrylate Hydrogels with A Camphorquinone-Trithanolamine Photoinitiator*** *(ACS Macro Letters in Review, co-first author)*
The novelty of our project is that we introduce blue light photoinitiator system (Camphorquinone-Trithanolamine) to polymerize PEGDA hydrogels on microfluidic chips while the most widely used photoinitiator is irgacure. And with digital masks device (DMD), we are able to make tiny hydrogels with different shapes (hundreds of microns in dimension).

•***Triggering DNA Diffusion-Reaction and UV Photo-Uncaging Reaction in Digital Photolithographic Patterned Poly (Ethylene Glycol) Diacrylate Hydrogels***
We want to demonstrate that the hydrogel we fabricated with the method in our previous protocol enables us to trigger not only strand-displacement reaction but also further photo-uncage reaction. DNA molecules designed with a UV photo-uncage site are anchored onto the gel, and complimentary DNA strands diffuse in. Enzyme-free DNA reaction first takes place and then DNA-based strand-displacement is triggered by UV light in certain specific domain of the hydrogel.

•***Soft Material Programming Through the Spatiotemporal Release of Oligonucleotides***

Our materials use enzyme-free DNA-based strand-displacement to direct the sequential release of short oligonucleotides from spatial domains. Maskless photolithography enables the spatial sequestration of acrylate-modified short oligonucleotides within hydrogels at sizes of tens of microns. To control temporal release, a DNA reaction-cascade that relies on toehold mediated strand displacement was implemented. The tuning of reactant concentrations and toehold sizes allows for the temporal control of DNA release.

PUBLICATION

• **ACS Macro Letters in review**
Title: *A digital maskless photolithographic patterning method for poly(ethylene glycol) diacrylate hydrogels with a camphorquinone-triethanolamine photoinitiator*
Author: Dorsey, Phillip; Rubanov, Moshe; Wang, Wenlu; Schulman, Rebecca
Manuscript ID: mz-2018-008188

PATENT

• *A Silicate Nanocomposite-Less Chrome Combination Tannage, Patent No.201610058007.8*

STANDARD TESTS

• **GRE: 159** (Verbal)**+170** (Quantitative) **+3.0**(Analytical)
• **TOEFL: 29** (Reading)**+ 25** (Listening)**+ 23** (Speaking)**+ 26** (Writing)**=103**

OTHER SKILLS

•**SOFTWARE:** Adobe Illustrator, Microsoft Office Suite, ImageJ, AutoCAD, Matlab

ADDITIONAL EXPERIENCES

•09/2013-05/2015
Community Volunteer Leader, providing community services regularly

•09/2014-01/2015

Part-time Shop Assistant, Chengdu C&A Fashion